ADVANCED MATERIALS
www.advmat.de

Materials Views
www.MaterialsViews.com

Small Adsorbate-Assisted Shape Control of Pd and Pt Nanocrystals

*Mei Chen, Binghui Wu, Jing Yang, and Nanfeng Zheng**

The shape control of noble metal nanocrystals is crucial to their optical properties and catalysis applications. In this Progress Report, the recent progress of shape-controlled synthesis of Pd and Pt nanostructures assisted by small adsorbates is summarized. The use of small strong adsorbates (e.g., I^-, CO, amines) makes it possible to fabricate Pd and Pt nanostructures with not only well-defined surface structure but also morphologies that have not been achieved by other synthetic strategies. The roles of small adsorbates in shape control of Pd and Pt nanocrystals are discussed in the Report. Also presented in the Report are unique optical and catalytic properties of several Pd and Pt nanostructures (e.g., ultrathin Pd nanosheets, concave Pt octapod, concave Pd tetrahedra), as well as their bioapplications, to demonstrate the power of using small strong adsorbates in the shape control of Pt and Pd nanostructures.

1. Introduction

The fascinating shape-dependent optical properties and surface-dependent catalytic properties are two key driving forces for the continuously growing research in the field of shape-controlled synthesis of noble metal nanocrystals in the last decades.[1–3] The optical properties of noble metal nanocrystals are mainly induced by the so-called surface plasmon resonance (SPR) phenomenon, a coherent oscillation of electrons taking place at the interface between a metal and a dielectric medium in response to the alternating electric field of incident light. The unique SPR properties of noble metal nanocrystals, which are dependent on the size, shape, assembly and also environment of the nanocrystals, have found use in a wide range of applications, such as optical sensing of biomolecules,[4] enhancing spectral signals,[5,6] probing catalytic reactions,[7] photothermal therapy,[8–11] etc. As a collective property, SPR of noble metal nanocrystals is more sensitive to the morphology of noble metal nanocrystals rather than their exposure surfaces. As a surface property, in contrast, catalysis concerns more on the surface structure of noble metal nanocrystals. In the synthesis of noble metal nanocrystals, however, shape control and surface control are essentially two closely related issues.

Based on the feature of their SPR and catalytic properties, noble metal nanocrystals can be classified into two distinct categories, the coinage metals (i.e., Ag and Au) and the Pt-group metals. On one hand, nanocrystals of the coinage metals possess tunable SPR in a wide spectral region, but have limited use in catalysis. On the other hand, nanocrystals of Pd and Pt find much wider applications as catalysts, but do not display SPR properties as good as those of Ag and Au nanostructures. Such a distinction is mainly due to the intrinsic difference between the coinage metals and the Pt-group metals. The surface-dependent catalysis of noble metal nanocrystals is mainly caused by the different adsorption behaviors of catalysis molecules on various facets. The surface energy difference of different Pd and Pt facets is typically larger than that of corresponding Ag and Au surfaces,[12] making the catalysis of Pd and Pt more sensitive to the surface difference than that of Ag and Au. With no doubt, the rather small surface energy difference between different surfaces of Ag and Au is beneficial to shape Ag and Au nanocrystals in more diverse morphologies, because the small energy barrier between different morphologies can be easily overcome by fine-tuning the reaction parameters. In the past two decades, indeed, the shape-controlled synthesis of Ag and Au nanocrystals has received great success,[2,3] resulting in the appearance of a large number of different-shaped nanocrystals for various applications. Many of the obtained Au nanocrystals are even bound by high-index facets.[13–16] High-index facets are highly open surfaces and promising for catalysis applications. However, the surface-dependent catalysis performances of Ag and Au nanocrystals were less explored. In contrast, Pt and Pd nanomaterials with well-defined surface structures have been widely applied for the surface-dependent catalysis studies under real catalysis conditions. During the past decades, metal single-crystal surfaces have been widely adopted by surface scientists as model catalysts to systematically study the effect of surface structure on catalysis reactions, such as ammonia synthesis, isomerization of light alkanes, hydrogenolysis of alkanes and so on.[17–19] In order to gain a clear picture on the surface structure effect, such studies were typically performed in ultrahigh vacuum (UHV), leading to the pressure and material gaps between many model catalysis studies and real catalysis.

M. Chen, B. H. Wu, Dr. J. Yang, Prof. N. F. Zheng
State Key Laboratory for Physical Chemistry of Solid Surfaces
and Department of Chemistry
College of Chemistry and Chemical Engineering
Xiamen University
Xiamen 361005, China
E-mail: nfzheng@xmu.edu.cn

DOI: 10.1002/adma.201104145

Owing to the high surface-area-to-volume ratio, nanomaterials are ideal materials to bridge these gaps in heterogeneous catalysis.[20–22] Although shape controlled synthesis of colloidal Pt crystals was already achieved in 1996,[23] the challenge still remains to precisely control the surface structures of nanocrystals of Pt-group metals. The demonstration of shape-dependent catalysis behaviors is mainly limited to nanocrystals bound by low-index surfaces (e.g., {111}, {100}).[24–27]

Since several excellent review articles have appeared recently to cover a broad range of topics related to the shape-controlled synthesis of noble metal nanocrystals,[2,3,28,29] this Report is not intended to be comprehensive but to highlight the recent progress of the shape-controlled synthesis of Pd and Pt nanocrystals using small adsorbates. Currently, polymers, surfactants, and large fatty ligands (e.g., amines, carboxylic acids, phosphines) are three major types of capping agents widely used in the synthesis of Pd and Pt nanocrystals. However, the use of these capping agents leads to inevitable consequences on catalysis applications of the prepared nanocrystals. On one hand, due to polyvalency effect, the strong binding of polymeric capping agents on the surface of nanocrystals induces the difficulty in cleaning them from the surface. On the other hand, fatty molecules on the surface make nanocrystals usually dispersible only in non-polar organic solvents. Even worse is the presence of van der Waals attractions between fatty molecules or surfactants, which makes a close-packed organic shell preventing the reactants from accessing the metal surface. Therefore, the Pd and Pt nanocrystals capped by polymers, surfactants, and fatty ligands have to be cleaned before catalysis applications. However, it is still unclear whether the cleaning processes would reconstruct the surface of as-made nanocrystals, which is deleterious to the goal of studying surface-dependent catalysis using shape-controlled nanocrystals. In contrast, the use of small strong adsorbates in the shape-controlled synthesis of Pd and Pt nanocrystals allows us to avoid such an embarrassing situation. While facilitating the surface control by specific strong adsorption, the built-up chemisorbed layer is not close-packed and thick enough to prevent the access of other molecules, which is beneficial to the adsorbate removal and thus catalysis applications of the prepared nanocrystals. More importantly, the adsorption of small adsorbates on the surface of nanocrystals can be investigated by various techniques, helping us to correlate the adsorbate-surface structure relationship for the predictive design and synthesis of Pd and Pt nanocrystals for demanded applications.

In this Report, we first discuss the relationship between surface structure and morphology of noble metal nanocrystals, and the common strategies in their shape control. Several examples are then given to illustrate and discuss: 1) how small adsorbates control the surface structure of Pd and Pt nanocrystals (Section 4); 2) how kinetic factors enrich the shape of nanocrystals with a specific surface (Section 5); 3) the roles of small adsorbates in the shape control other than the surface adsorption (Section 6). Unique optical and catalytic properties of several Pd and Pt nanostructures (e.g., ultrathin Pd nanosheets, concave Pt octapods, concave Pd tetrahedra) are also presented to demonstrate the power of small strong adsorbates in creating Pd and Pt nanostructures that are not easily accessible by other preparation methods.

Professor Nanfeng Zheng received his Ph.D. from University of California at Riverside in 2005. After two-year postdoctoral work at University of California at Santa Barbara, he moved to Xiamen University as a full professor in 2007. He is currently a Changjiang Chair professor at Xiamen University. In 2009, he received the Distinguished Young Investigator Award from NSF-China. His research interests focus on advanced functional materials for both fundamental research and practical applications, particularly in the fields of catalysis and biology.

Finally, conclusions and prospects are summarized to discuss the challenges of the shape-controlled synthesis of Pd and Pt nanocrystals using small adsorbates.

2. Relationship Between Surface Structure and Morphology

Face-centered cubic (fcc) metals have their atoms close-packed in an ABCABC stacking sequence along [111]. Although the coordination number (CN) of atoms inside an fcc nanocrystal is 12, the CN of surface atoms varies with the surface structure. Atoms on {111}, {100} and {110} surfaces, the three so-called low-index surfaces, have a CN of 9, 8, and 7, respectively. The planar densities of these three surfaces decrease in the order of {111}>{100}>{110}. The clean low-index surfaces of an fcc metal have therefore the surface energies in the order of $\gamma_{\{111\}} < \gamma_{\{100\}} << \gamma_{\{110\}}$.[12,30] The crystallographic planes with higher Miller indices (*hkl*) having at least one index being larger than 1 are called high-index surfaces. Compared with low-index surfaces, particularly {100} and {111}, the high-index facets of an fcc metal are featured by a high density of low-coordination step atoms (CN = 7) and/or kink sites (CN = 6) and thus exhibit enhanced activity in many catalysis and electrocatalysis reactions.[31,32] However, the high-index facets are generally difficult to be obtained by conventional chemical methods.

For fcc metals, the morphology and surface of their nanocrystals are closely related. As shown in **Figure 1**a, the shape of typical single-crystalline polyhedra enclosed by various crystalline facets is often summarized and illustrated by a stereographic triangle. In the triangle, the polyhedral crystals (i.e., octahedron, rhombic dodecahedron) enclosed by the three basal facets (i.e., {111}, {100}, {110}, respectively) are located at the three vertexes. While polyhedra respectively bound by the three different types of high-index surfaces [i.e., {*hk*0}, {*hkk*}, {*hhl*} ($h \neq k \neq l \neq 0$)] are distributed at the three edges of the triangle, polyhedra enclosed by {*hkl*} ($h \neq k \neq l$) are

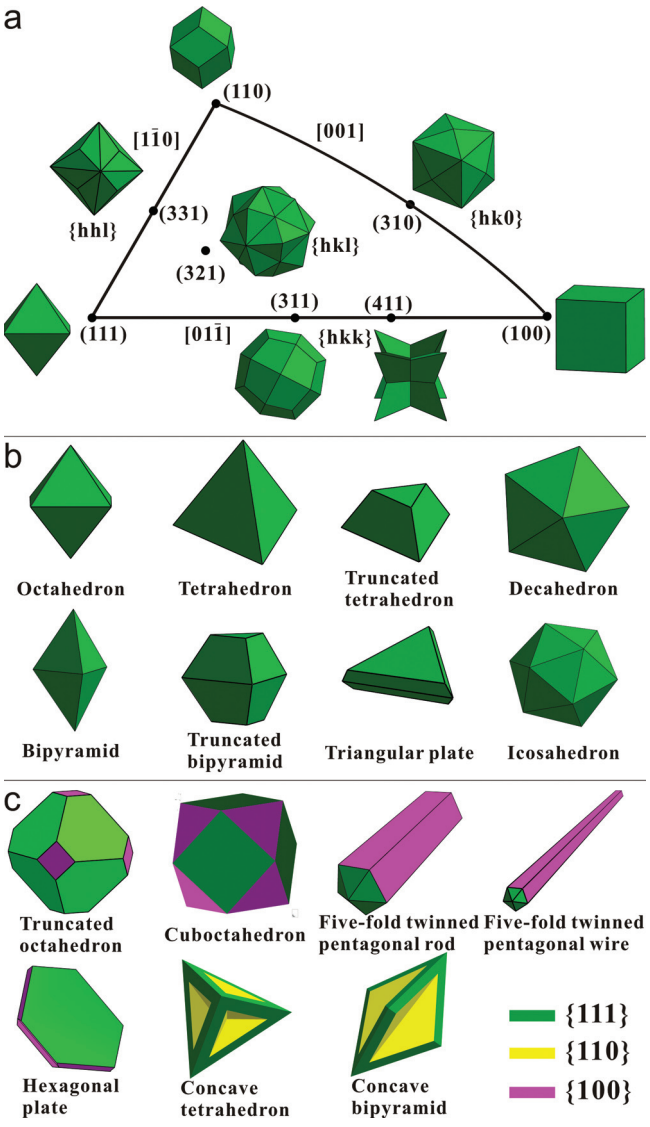

Figure 1. Typical morphologies of fcc metal nanocrystals. a) Stereographic triangle single-crystalline polyhedra of fcc metal enclosed by various types of crystal planes. b) Polyhedra enclosed by {111} facets. c) Polyhedra enclosed by mixed facets.

located inside the triangle. Examples of single-crystalline polyhedral nanocrystals of fcc metals that have been successfully synthesized are tetrahexahedron (THH)[14,33,34]/concave cube[15]/truncated ditetragonal prism[35,36] enclosed by {*hk0*}, trisoctahedron by {*hhl*},[13] octapod by {*hkk*},[37] and concave hexoctahedron by {*hkl*}.[38] The presence of twinned boundaries can significantly enrich the morphology of nanocrystals enclosed by a specific surface. For example, as shown in Figure 1b, although single-crystalline polyhedra enclosed by {111} are limited to octahedron, tetrahedron and truncated tetrahedron, a large variety of {111} enclosed polyhedra having twinned boundaries have been prepared. These twinned polyhedra include single twinned trigonal bipyramid/truncated bipyramid, five-fold twinned decahedron, and multiply-twinned icosahedron. Moreover, the shape of nanocrystals of fcc metals can be further enriched by having mixed facets (Figure 1c). For instance, cuboctahedron, truncated octahedron, five-twinned nanorod/nanowire, and hexagonal plate are enclosed by a mixture of {111} and {100} facets. Both {111} and {110} are revealed in the concave tetrahedron and concave bipyramid.[39]

3. Common Strategies in the Shape-Controlled Synthesis of Noble Metal Nanocrystals

Taken together, Section 2 tells that the surface together with the twinned boundaries/defects in nanocrystals of an fcc metal determines the morphology of the nanocrystals. To better control the shape of noble metal nanocrystals, the following two important issues have to be considered: 1) how to control the surface structure of the nanocrystals, and 2) how to induce the formation of twinned boundaries or defects in the nanocrystals. Due to similar stabilization energy, small seeds having either single crystalline, single or multiple twinned feature are usually presented in the same reaction simultaneously. The balance between surface energy and strain energy caused by twinned boundaries, and between energetics and kinetics, often determines nucleation and growth of the nanocrystals, and thus the final shape of the nanocrystals. The following are several example strategies showing how thermodynamic and kinetic parameters of a reaction control the shape of the nanocrystals.

3.1. Selective Surface Capping

A large variety of surfactants, polymeric molecules, and recently small adsorbates, and biomolecules have been found to play certain roles in the shape control of noble metal nanocrystals. For instance, cationic surfactants, such as cetyltrimethylammonium bromide (CTAB), facilitate the controlled synthesis of Au nanorods.[40] In the polyol synthesis of noble metal nanocrystals, poly(vinyl pyrrolidone) (PVP) has been revealed as an effective capping polymer to control the formation of different-shaped nanocrystals.[2,41] Although the selective production of nanocrystals with certain shape can be achieved by selective adsorption of surfactants or polymeric molecules onto specific surfaces, it is still obscure how these capping agents selectively bind on the specific metal surfaces. In the past several years, small strong adsorbates have also emerged as a class of very effective surface controllers in the synthesis of noble metal nanocrystals, particularly Pd and Pt. For instance, Yang *et al.* demonstrated that NO_2 stabilized Pd {111}. Increasing the ratio of NO_2 to Pd in the synthesis led to an increasing ratio of {111} to {100} in the obtained Pd nanocrystals.[42] Ag^+ ions were revealed able to facilitate the formation of Pt nanocrystals bounded by larger areas of {111} facets.[43] The selective binding of halides on Pd/Rh {100} promoted the formation of Pd nanocubes/nanobars[44,45] and Rh nanocubes.[46] CO preferred to adsorb on Pd {111} to facilitate the production of Pd nanosheets.[47]

3.2. Oxidative Etching

In the synthesis of noble metal nanocrystals, twinned structures frequently appear along with single crystals. It is somewhat a challenge to selectively prepare pure twinned or single nanocrystals. Extensive work has been reported on the controlled synthesis of noble metal nanostructures by using oxidative etchants, like Fe^{3+}, O_2/Cl^-, NO_3^-, NH_4OH/H_2O_2, $NH_4OH/H_2O_2/CrO_3$ mixture, etc.[48–52] While the presence of twinned boundaries makes twinned particles more prone to being oxidatively etched by an appropriate oxidant, the absence of twinned boundary defects makes single-crystalline particles more resistant to the oxidation. Particularly when the particles are small, such a reactivity difference between twinned and single-crystalline particles allows selectively eliminating the twinned seeds and leaving only single-crystalline seeds for the further growth process. For example, with the use of O_2/Cl^- in the polyol synthesis of Ag nanocrystals, high-yield production of single-crystalline has been achieved.[49] In contrast, blocking the oxidative etching is an option to produce particularly twinned nanocrystals. Five-fold twinned, starfish-like Rh nanocrystals were synthesized by eliminating oxidative etching with a Cl^- free precursor.[53] O_2/Cl^- and Fe^{3+} were claimed as oxidative etchants to reduce the reduction rate of Pd(II) precursors for the formation of Pd nanoplates.[54]

3.3. Seeded Growth

Considering that nucleation and growth are the two very important stages in the controlled synthesis of nanocrystals, the method of seeded growth has been developed to chemically isolate the nucleation and growth steps. In the method, pre-made small nanocrystals with well-defined shape were used as the seeds for the growth step. Such a strategy has been demonstrated effective in the synthesis of many unique noble metal nanocrystals. For example, the use of small Au nanoparticle seeds allows the production of a variety of Au nanostructures including nanorods with a wide range of aspect ratio.[40] Furthermore, pre-made nanocrystals with well-defined shape have been applied to study how the shape and composition of the seeds influence the shape of final nanocrystals.[42,55,56]

Even with the significant progress in the shape controlled synthesis of colloidal Pd and Pt, as mentioned above, the Pd and Pt nanocrystals prepared by wet-chemistry methods are usually enclosed by low-index surfaces (e.g., {111},{100}).[2,3,28,29,57] The shape-controlled synthesis of Pd and Pt nanocrystals still faces the following challenges: 1) Many syntheses of Pd and Pt nanocrystals involved the use of different additives. But the roles of the additives were poorly understood.[2,29] 2) Although nanocrystals enclosed by high-index Pd and Pt facets have been prepared by the seeded growth using pre-made high-index faceted Au nanocrystals as the seeds,[56,58–61] and electrochemical method,[33,62,63] the direct wet-chemical synthesis of Pd and Pt nanocrystals with high-index exposure surfaces remains difficult. 3) Pd and Pt nanocrystals usually display poor SPR properties. Can unique Pd and Pt nanostructures be prepared to exhibit promising optical properties?

4. Surface Structure Control and Unique Properties of Pd and Pt Nanocrystals Induced by Specific Adsorption of Small Adsorbates

Recently, our group has focused on the use of small strong adsorbates as shape control agents in the synthesis of Pd and Pt nanocrystals.[37,39,45,47,64,65] Studies from our group and others have clearly demonstrated that the strong adsorption of several adsorbates, like I^-, CO and amines, could serve as an effective factor to enrich not only the surface structure but also the shape of Pd and Pt nanocrystals. In the following sections, several examples are used to discuss how different small adsorbates control the shape of Pd and Pt nanocrystals mainly from thermodynamic and kinetic aspects.

4.1. Formation of Pd Nanocubes Assisted by Halide Anions

Many studies in surface science revealed that halides, particularly Br^- and I^-, adsorb tightly on clean single-crystalline Pd surfaces.[66,67] The strong binding of halides on metallic Pd surfaces suggests that halides could potentially play an important role in the chemical synthesis of Pd nanocrystals by changing the surface energy of different Pd facets. However, the studies on the effect of halide anions on the shape-controlled synthesis of Pd nanocrystals were not done until 2007 by Xia.[44] By introducing Br^- into the polyol synthesis containing Na_2PdCl_4 as the Pd precursor and PVP as the capping agent in ethylene glycol, nice Pd nanocubes and nanobars enclosed by {100} facets were successfully obtained (**Figure 2**). In comparison, the absence of Br^- in the synthesis led to the formation of cuboctahedral nanocrystals enclosed by a mix of {111} and {100} facets. For fcc metals, the surface energy of {100} facets free of any adsorbates is higher than that of {111}. Therefore, Pd nanocubes and nanobars are not the energetically favored geometries during the synthesis. The preferential growth of nanocrystals enclosed by {100} in the presence of Br^- was attributed to the selective and strong adsorption of Br^- on Pd {100}. Even after extensive washing with water, the presence of a significant amount of Br^- on the surface of the as-prepared Pd nanobars was revealed by EDX and XPS measurements.[44]

What remained unclear in the polyol synthesis is why replacing Br^- with either Cl^- or I^- did not yield nanocrystals fully enclosed by {100} facets (Figure 2a, 2c). Since Cl^- is a weaker adsorbate than Br^-, it is easy to understand why the presence of Cl^- did not lead to the formation of nanocubes or nanobars. But the failure to prepare nanocubes in the presence of I^- cannot be interpreted simply by thermodynamics. Studies by surface scientists have demonstrated that the chemisorption ability of halides on single-crystalline Pd surface increases in an order of $Cl^- < Br^- < I^-$.[66] From the view point of energetics, the strong chemisorption of I^- on Pd (100) should make it easier to prepare nanocrystals enclosed with {100} facets. Interestingly, when the reaction system was shifted from polyol to N,N-dimethyl formamide (DMF), Zheng and coworkers obtained Pd

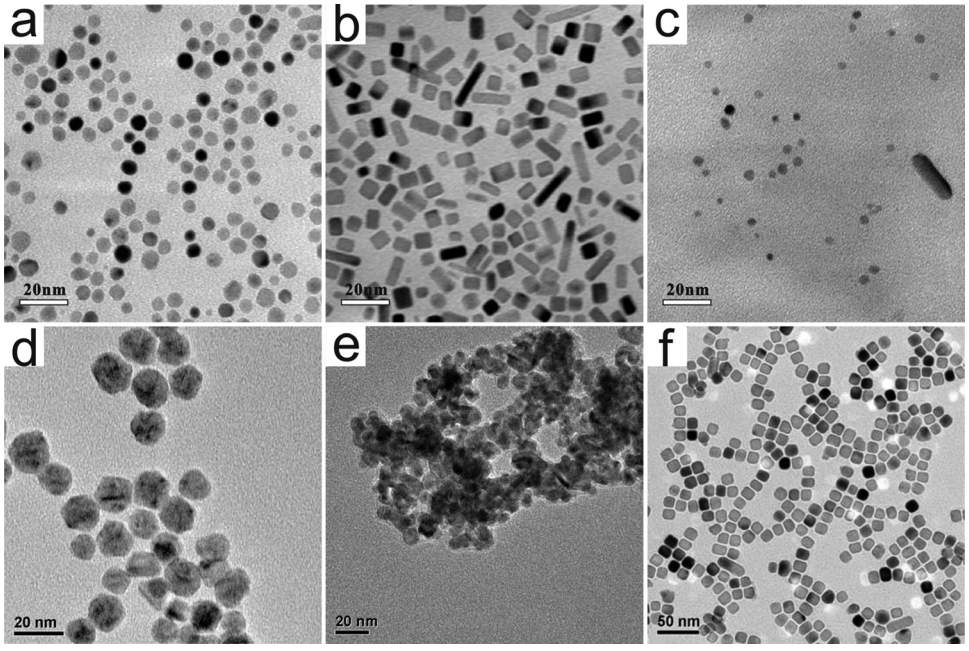

Figure 2. TEM images of Pd nanocrystals prepared in the presence of different halides: a,d) Cl^-, b,e) Br^-, and c,f) I^-. a–c) Pd nanocrystals synthesized in a mixture of ethylene glycol and water, with Na_2PdCl_4 as precursor and PVP as capping agent. d–f) Pd nanocrystals synthesized in DMF, with $Pd(acac)_2$ as precursor and PVP as capping agent. a–c) Reproduced with permission from ref. [44]. Copyright 2007 American Chemical Society. d–f) Reproduced with permission from ref. [45].

nanocubes only in the presence of I^-.[45] In their system, Pd(II) acetylacetonate [$Pd(acac)_2$] was applied as the Pd precursor to examine the effect of halides without the influence of Cl^- from the precursor, and poly(vinyl pyrrolidone) (PVP) was still used as the capping agent. To evaluate the effect of different halides on the shape-controlled synthesis of Pd nanocrystals, the mixtures of $Pd(acac)_2$, PVP and aqueous solution of sodium halide (i.e., NaI, NaBr, NaCl, NaF) in DMF were heated at 150 °C for 8 h. As clearly illustrated in the TEM images of the collected products (Figure 2d–f), only the reaction in the presence of I^- yielded Pd nanocubes. The Pd nanocubes were single crystallites with a uniform size of 13 nm. The production of Pd nanocubes enclosed by {100} facets in the presence of I^-, although different from the observation in the polyol synthesis, is expected from viewpoint of thermodynamics. In comparison, the reactions in the absence of halide yielded semiregular polyhedral nanoparticles with a size of about 50 nm. These particles were featured by their multiply twinned structure which was also presented in the particles prepared from the reactions where NaI was replaced by an equal amount of NaCl (Figure 2d), or NaBr (Figure 2e). It should be pointed out that the importance of certain halide on the synthesis of nanocubes of fcc metals was also recognized by other groups in the literature. For example, sub-10 nm Pd nanocubes were prepared by introducing NaBr in the presence of PVP and sodium lauryl sulfate in aqueous solution.[68] Rh nanocubes were successfully prepared when Br^- was added in the synthesis.[46,69] The combined use of Br^- and I^- were required to yield alloy PtPd nanocubes.[70]

The preferential binding of halides on {100} surfaces offers a potential method to selectively produce nanocubes of fcc metals by lowering the surface energy of the exposed surface. Thermodynamically, the stronger surface adsorbates would reduce more surface energy of the facets where they adsorb. However, the growth activity of nanoparticles is generally repressed by the strong adsorption of small adsorbates on their surface. In the presence of strong {100} adsorbate I^-, Pd nanocubes were obtained in the DMF system but not synthesized in the polyol system, indicating the importance of reaction system in making the specific surface adsorption of small adsorbates as the main contributor for the surface control.

4.2. Preparation of Ultrathin Pd Nanosheets Aided by Carbon Monoxide

Based on the result that high-quality Pd nanocubes were obtained using the strong {100} adsorbate I^- as the surface controller, one would be eager to know the possibility to apply other strong adsorbates to control the surface structure of Pd nanocrystals. One immediate idea that easily comes to mind is to use CO. In many catalysis studies, CO is frequently recognized as a common poisoning agent of Pd and Pt catalysts due to the strong adsorption of CO on their surfaces which could prevent other catalytic molecules from accessing the catalytic surfaces. Surface scientists have extensively studied the adsorption of CO on various surfaces of Pd under vacuum conditions and also drawn the conclusion that CO exhibits strong adsorption on Pd surfaces.[71–73] Compared with halides, the beauty of CO adsorbate is that CO molecules adsorbed on Pd can be removed by applying a high temperature or an electrochemical oxidation potential, which makes it easy to clean the surface of the as-prepared CO-capped Pd nanocrystals.

Experimentally, Zheng and coworkers introduced CO molecules into the synthesis of Pd nanocrystals by putting the reaction mixture under CO atmosphere.[47] The reaction contained $Pd(acac)_2$, a halide salt and PVP in a solvent (such as DMF, benzyl alcohol). As the reaction progressed, the color of the reaction mixture changed from yellow to light blue, and finally dark blue. The term "palladium black" extensively summarizes the optical properties of high-surface-area metallic Pd. The blue color is hardly observed in Pd nanostructures because most Pd nanostructures display no tunable SPR properties as discovered in Au and Ag nanostructures.[74] The ultrathin sheet-like feature of the Pd nanostructures prepared under CO atmosphere is the main reason why they exhibit the unique SPR properties to give the blue color. As revealed by TEM and SAED (**Figure 3**a–d), monodisperse Pd nanosheets with a thickness narrowly distributed at ~1.8 nm were obtained when the reaction mixtures contained halides. The nanosheets present a well-defined hexagonal shape with {111} facets as basal planes and {100} facets as side planes.

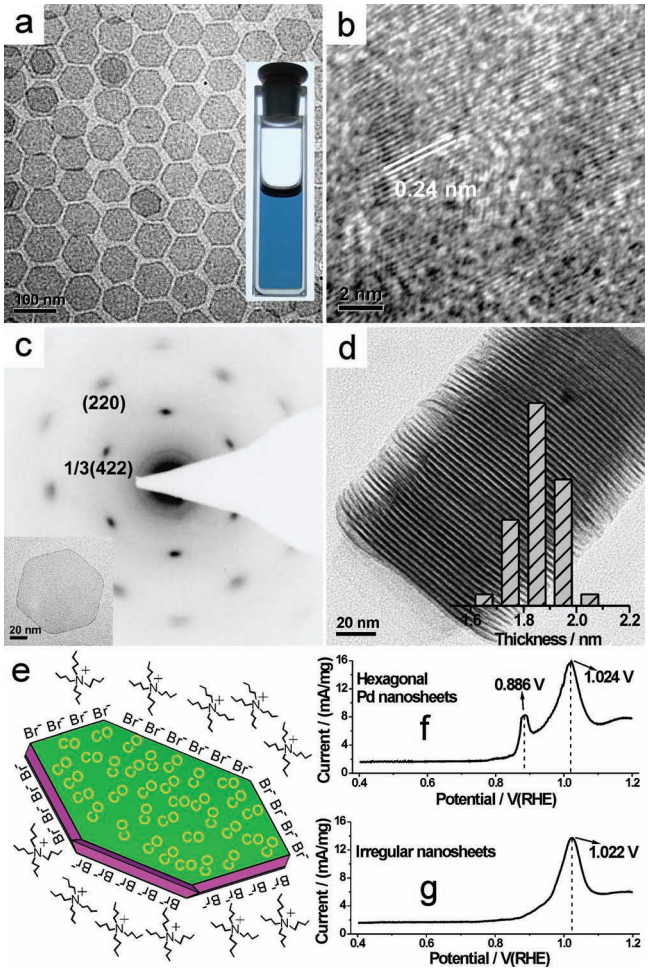

Figure 3. a) TEM image of ultrathin Pd nanosheets synthesized in the presence of PVP and TBAB in DMF aided by CO, right inset shows a photograph of dispersion of Pd nanosheets in ethanol. b) HRTEM image and c) SAED pattern of a single Pd nanosheet. d) TEM image of the assembly of Pd nanosheets which are perpendicular to the TEM grid, inset is the thickness distribution. e) Structure model of a hexagonal Pd nanosheet with CO molecules on the {111} facets, Br^- on the side {100} facets and NBu_4^+ as the counter ions. CO stripping voltammetry of 60 nm Pd nanosheets f) and irregular Pd nanosheets prepared with no halide g) in 0.1 M H_2SO_4 solution at a scan rate of 2 mV/s. Modified with permission from ref. [47]. Copyright 2011 Nature Publishing Group.

The exposure surfaces of the nanosheets were also identified by electrochemical CO stripping measurements, a powerful technique to distinguish the binding energies of CO on various Pd surfaces.[75] Only a major peak attributed to Pd (111) (1.02 V versus RHE) was observed in the CO stripping profiles on the Pd nanosheets right after centrifugation. When external CO was introduced, an additional small peak corresponding to CO stripping on Pd (100) was developed. These results suggested that CO molecules were tightly bound on the lower and upper {111} planes and halides were associated on the six side {100} planes of the nanosheets (Figure 3e). The halide adsorption on Pd (100) was not as strong as the adsorption of CO on Pd (111). During the synthesis, the six halide-bound {100} facets were the growth active sites at which the freshly reduced Pd atoms/clusters were added. Such a growth model was consistent with the observation that the edge length of the nanosheets increased with reaction time while their thickness remained unchanged (1.8 nm) before the depletion of the precursor. After the Pd nanosheets were purified from the reaction mixture containing large amount of halides, the halides adsorbed on Pd {100} were ticked out by CO to develop the (100) CO stripping peak (0.89 V versus RHE) (Figure 3f). These CO stripping experiments further demonstrated that the presence of CO and halide was responsible for forming (111) and (100) planes, respectively. The important role of halide in forming (100) facets is consistent with the observation of Pd nanocubes formation in the presence of Br^- or I^-.[44,45] Such a halide effect was also verified by the CO stripping profile of the irregular Pd nanosheets obtained from the reactions without halide in which only one stripping peak corresponding to Pd (111) was revealed (Figure 3g).

The SPR properties of metal nanostructures are typically dependent on structure, size and how they are aggregated. The chemisorption of halide on Pd nanosheets makes them negatively charged so that they can be freestanding and highly dispersible in solutions. Such a feature allows us to well correlate their SPR properties with the size. As shown in **Figure 4**a, the as-prepared Pd nanosheets with the thickness fixed at 1.8 nm exhibit well-defined size-dependent and tunable SPR absorption peaks in the near infra red (NIR) region. It has been previously reported that the Pd nanoplates with the thickness of ~5 nm displayed only broad SPR peaks in the visible region.[54] As suggested by the calculations of extinction spectra using the discrete dipole approximation (DDA) method, the ultrathin nature of the palladium nanosheets is essential to their unique SPR in the NIR region. More importantly, the nanosheets have high extinction coefficients in the NIR region. The extinction coefficient for the nanosheets with an edge size of 41 nm was measured to be 4.1×10^9 M^{-1} cm^{-1} at 1045 nm, comparable to those reported for gold nanorods. Owing to their strong NIR SPR absorption, the ultrathin palladium nanosheets prepared by the use of CO display remarkable photothermal effect that can effectively convert NIR irradiation into heat (Figure 4b). Unlike Au/Ag nanostructures displaying strong NIR SPR absorption, the Pd nanosheets appear to be highly stable and do

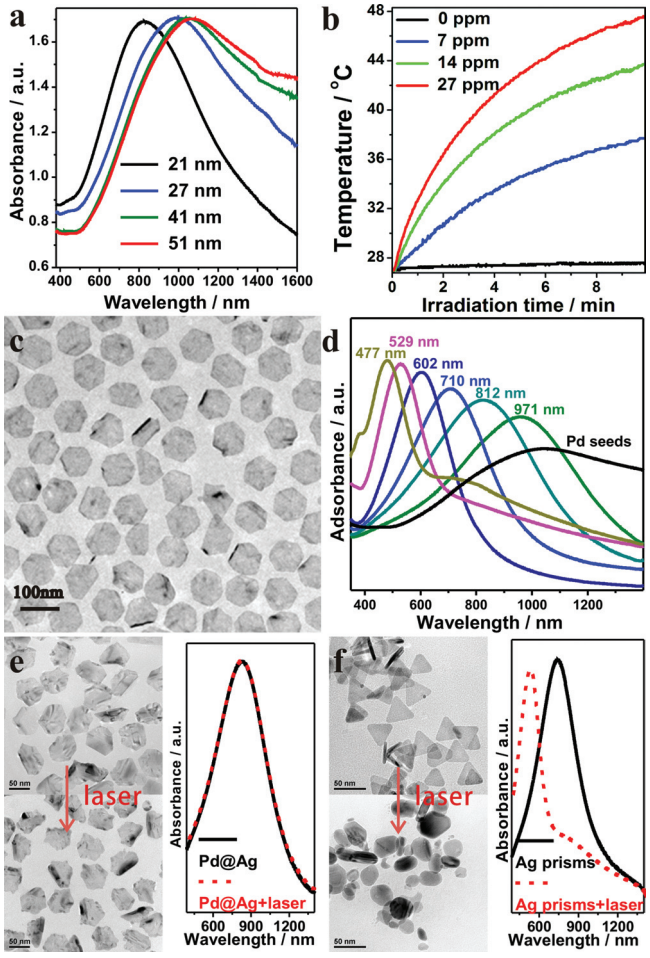

Figure 4. a) Absorption spectra of Pd nanosheets with different average edge lengths. b) Photothermal effect of 41 nm Pd nanosheets with different concentration after 10-min-irradiation by a 1-W laser. c) Representative TEM image of Pd@Ag core-shell bimetallic nanoplates. d) Tunable plasmon bands of Pd@Ag nanoplates by varying the molar ratio of $AgNO_3$/Pd. e,f) Photothermal stability of Pd@Ag nanoplates e) and Ag nanoprisms f) upon irradiation for 30 min with a 2-W, 808 nm laser. In e) and f), top-left and bottom-left TEM images were obtained before and after the laser irradiation respectively, while the right side absorption spectra show the SPR changes. a, b) Reproduced with permission from ref. [47], copyright 2011 Nature Publishing Group. c-f) Modified with permission from ref. [76].

not melt into spherical particles by the heat created by the NIR irradiation. Starting from these ultrathin Pd nanosheets, a class of core-shell Pd@Ag nanostructures integrating both tunable SPR properties and photothermal stability were also successfully obtained by coating the nanosheets with Ag at different thickness (Figure 4c, 4d).[76] The core-shell Pd@Ag nanoplates display significantly enhanced photothermal stability as compared with pure Ag nanostructures (Figure 4e, 4f). Their NIR SPR properties of the as-prepared Pd@Ag nanoplates were greatly preserved even after irradiation of high-power laser.

Owing to the deep tissue penetrating nature of NIR radiation, photothermal therapy using NIR laser has recently emerged as a new candidate technique for cancer treatment. The remarkable NIR photothermal effect and stability make the ultrathin Pd nanosheets promising for cancer therapy using NIR irradiation. Although the ultrathin Pd nanosheets exhibit excellent biocompatibility and NIR photothermal cell-killing efficacy, their application in photothermal therapy meets the problem that the ultrathin nature of the Pd nanosheets prevents them entering cells effectively, which however provides a nice system to study the thickness-dependent cells' uptake efficiency. For example, silica coating followed by surface modification by amino groups has been demonstrated able to increase the cells' uptake of the Pd nanosheets by 13 times.[77] To be used in practical therapy, required are more extensive works on how Pd nanosheets can be taken up by cancer tissues more efficiently and also excreted from body.

It should be pointed out that CO has also been used for the synthesis of Pd nanostructures by other groups.[78–80] For example, Pd nanosheets were also prepared in the emulsions or mesophases formed by CTAB, water and toluene containing Pd complexes.[78] In the CTAB method, the coordinated use of both CTAB and CO was claimed critical for the formation of thin plate structures. The as-reported Pd nanosheets were somewhat heavily aggregated and did not exhibit well-defined SPR peak. In the synthesis involved the use of amphiphilic hyperbranched polymers, the importance of the polymers in producing Pd nanosheets was also suggested.[79] Prior to our work, the role of CO in the surface control of the Pd nanosheets was not well recognized. Although the roles of CO and halide in the synthesis of Pd nanosheets have been well understood, there is still no clear answer to why the adsorption of CO confines the growth of the nanosheets to be 1.8-nm thick. Many previous studies have demonstrated that, because of the electronic confinement effect, metallic thin films grown on semiconductor substrates can have several preferred thicknesses.[81] The reason for the preference of only one thickness in the growth of palladium nanosheets remains unclear and requires further investigation.

4.3. Formation of Pt Nanocubes Induced by CO Adsorption

Pd and Pt are in the same group of periodic table and both display strong CO adsorption. With the surface confinement of CO, ultrathin Pd nanosheets have been obtained.[47] What will happen if CO is introduced in the synthesis of Pt nanocrystals? In turning back to literature, the controlled synthesis of Pt nanocrystals using CO-containing compounds has been reported by several groups. Back to 2007, Sun *et al.* prepared Pt nanocubes by introducing a trace amount of $Fe(CO)_5$ and revealed the important role of $Fe(CO)_5$ in the formation of Pt nanocubes (**Figure 5**a).[82] Fang's group reported the synthesis of nanocubes of Pt and Pt_3M (M = Co, Fe, Ni) by having $W(CO)_6$ in the reactions (Figure 5b).[83] The molecular ratio of $W(CO)_6$ to $Pt(acac)_2$ was as high as 2.8. Pt nanocubes were also prepared in the presence of trace $Co_2(CO)_8$.[84] No formation of Pt nanocubes was observed when $Co_2(CO)_8$ was replaced by other Co sources. Although the zero-valent metal in the metal carbonyls was considered to play an essential role in the synthesis, possible role of CO decomposed from the carbonyls during the reaction was entirely ignored. Furthermore, it should be pointed out that the addition of metal carbonyls might introduce impurities, such as alloy formation in Pt or adatoms on Pt surfaces, which could result in a more complex surface structure.

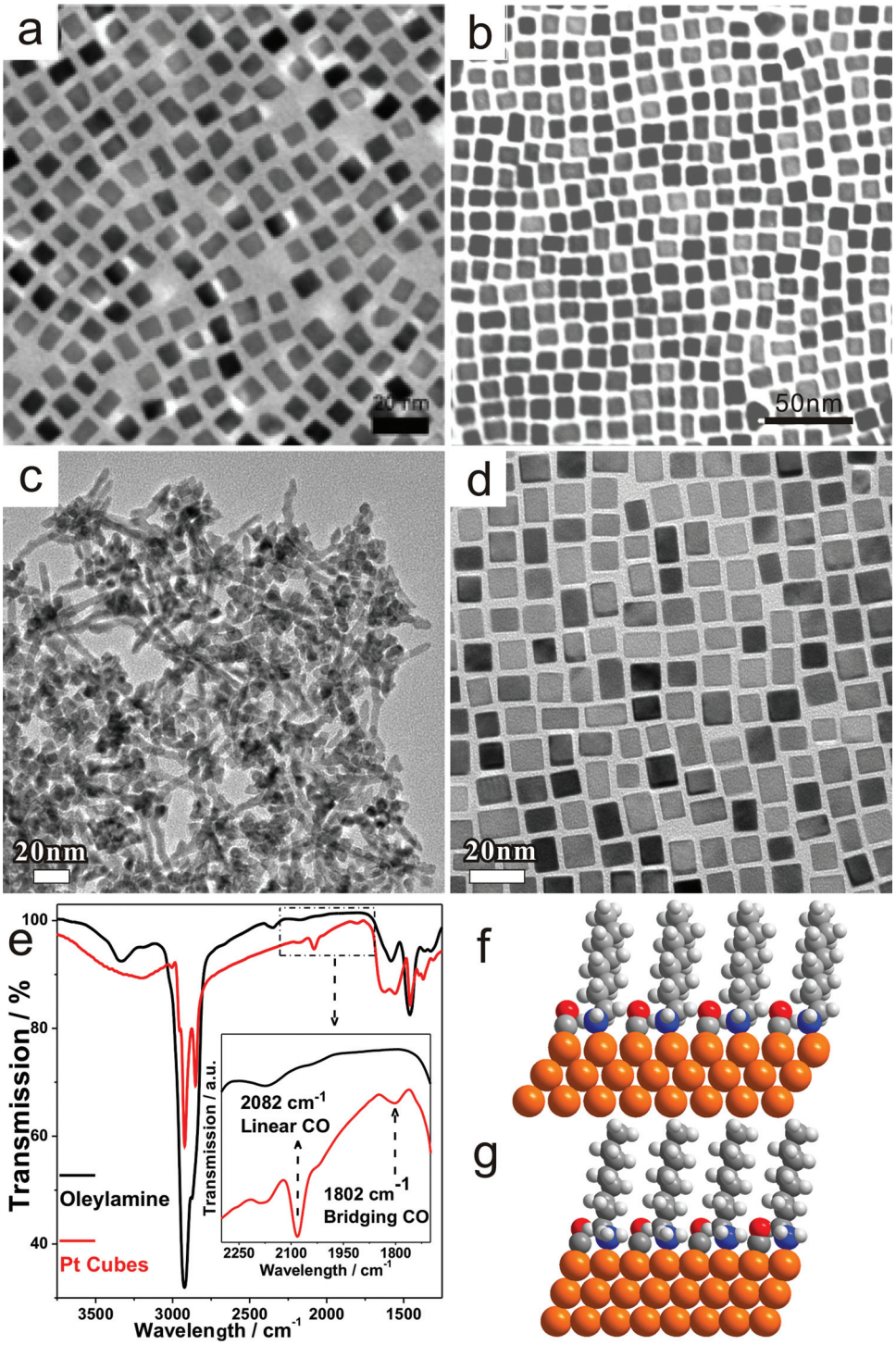

Figure 5. a) TEM image of Pt nanocubes prepared with a trace amount of $Fe(CO)_5$ (reproduced with permission from ref. [82], copyright 2007 American Chemical Society). b) TEM image of Pt nanocubes prepared with the use of $W(CO)_6$ (reproduced with permission from ref. [83], copyright 2009 American Chemical Society). c) TEM image of Pt nanocrystals prepared without CO while Pt nanocubes in d) were synthesized under CO flow. e) IR spectra of Pt nanocubes prepared in 4:1 OAm/OLA mixed solvent. f,g) Structure models of (100) facet f) and (111) facet g) co-adsorbed by CO/amine by spin-polarized DFT calculations. c–e): reproduced with permission from ref. [85], copyright 2011 Royal Society of Chemistry.

Considering the above issues, Zheng *et al.* introduced commercial pure CO gas to study possible role of CO in shape-controlled synthesis of Pt nanocrystals.[85] In the absence of any metal carbonyl or CO, the thermal decomposition of $Pt(acac)_2$ in the 4:1 oleylamine/oleic acid mixed solvent at 180 °C led to the formation of Pt nanodendrites (Figure 5c). But when a

CO gas flow (~30 mL/min) was applied on the surface of the reaction solution, the formation of high-quality Pt nanocubes was observed (Figure 5d).[85] The nanocubes were also readily prepared by lowering the CO flow rate down to 3 mL/min or even using a CO gasbag. This result suggested the importance of CO in the formation of Pt nanocubes could originate from the strong binding of CO on Pt. FT-IR measurements were carried out to check the presence of CO adsorption on the as-made Pt nanocubes. While no CO adsorption was observed on Pt nanodendrites prepared in absence of CO, the as-prepared Pt nanocubes displayed an obvious CO band at 2082 cm^{-1} and a weak band at 1802 cm^{-1}, corresponding to linear and bridging CO respectively (Figure 5e). The presence of oleylamine was revealed by the IR spectra too, meaning that Pt (100) surfaces were co-adsorbed by CO and amine (RNH_2). It should be noted that CO binding on Pt nanocubes was also detected when the nanocubes were synthesized by using $W(CO)_6$.

Based on the IR result that CO and amines were co-present on the surface of Pt nanocubes, various structure models of (100) and (111) capped by CO/amine were built for spin-polarized DFT calculations. The calculations showed that φ_{111} (surface energy per atom) is lower than φ_{100} by 0.26 eV when the surfaces are clean. The difference between φ_{111} and φ_{100} decreases to 0.20 eV and 0.15 eV after adsorbed by 0.25 monolayer (ML) RNH_2 and CO, respectively. The co-adsorption of RNH_2 (0.25 ML) and CO (0.25 ML) (Figure 5f, g) can reduce the difference between φ_{111} and φ_{100} to –0.02 eV. This result implies that (100) facet becomes more stable than (111) after the co-adsorption of CO and RNH_2 and explains why Pt nanocubes were readily prepared in the presence of CO.

The formation of Pt nanocubes assisted by CO was also reported by Murray's group.[86] Using CO as the reducing agent was claimed important to control the synthesis of Pt nanocubes in the presence of oleic acid and oleylamine. In their studies, gaseous CO was generated through dehydration of formic acid in warm concentrated sulfuric acid. CO was also found as an effective reducing agent to prepare ultrathin Au nanowires in the presence of oleylamine and uniform Pd nanocrystals in the presence of trioctylphosphine. The role of CO was mainly discussed by its unique feature as a reducing agent in controlling the reaction kinetics and therefore the morphology of the metal nanostructures. Besides the role as a reducing agent, however, no further insight was given to explain how CO induced the formation of Pt nanocubes. Again, by using CO as reducing agent, Yang and coworkers developed an effective method called GRAILS (gas reducing agent in liquid) to control the shape of Pt alloy (Pt-M, M = Co, Fe, Ni, Pd) nanocrystals.[87] Both cubic and octahedral Pt alloy nanocrystals were readily obtained by changing the reaction conditions. Similar phenomenon was observed by Fang *et al.* when $W(CO)_6$ was used as the reducing agent in the synthesis of Pt_3Ni nanocrystals.[88] In the controlled synthesis of Pt_3Mn nanocubes, metal carbonyl, $Mn_2(CO)_{10}$, was also used.[89] Interestingly, so far, there is no report on the synthesis of pure Pt octahedral nanocrystals using gaseous CO or metal carbonyl as the reducing agent. The different effect of CO on the formation of nanocrystals of pure Pt and Pt-M alloys could be due to the phenomenon of surface segregation.[90–93] Studies have demonstrated that the surface composition of Pt-M alloy nanocrystals could be varied by changing their surrounding environments. Such a surface composition variation might be the main cause for the different effect of CO on the shape control of pure Pt and Pt-M alloys. Further investigations are required to gain deep understanding over how CO controls the formation of different-shaped Pt-M nanocrystals under various conditions.

4.4. Amine-Assisted Synthesis of Pt Nanocrystals with High-Index Facets

As mentioned in Section 4.3, amines and CO co-adsorbed on the surface of the Pt nanocubes that were prepared in the co-presence of oleylamine and CO. This result implied that the adsorption of amines on metallic Pt surface is rather strong and comparable to that of CO. It is also well-known that the strong interaction between amines and cationic Pt are commonly presented in Pt complexes like *cis*-platinum. The unique feature of a Pt-amine bond is that the interaction is strong, but conditional. Pt-N coordination bonds are usually stable only under alkaline conditions and can be easily broken down by acids. One would expect that the surface of amine-capped Pt nanocrystals can be effectively cleaned by treating them with acids at low temperature. Such a method would help to prevent the surface reconstruction during the surface cleaning process, which is important for many structure-property correlation studies. Therefore, amines are good candidates to study the effect of small adsorbates on the surface control of Pt nanocrystals. In facts, fatty amines have been widely used in the synthesis of Pt nanocrystals.[29] The role of amines in the shape control was somewhat claimed but not well understood.

To simplify the synthesis system, in our studies, methylamine was first selected to evaluate the effect of amines in the synthesis of Pt nanocrystals. The reaction contained H_2PtCl_4, PVP and methylamine in DMF.[37] As illustrated in **Figure 6**, the reaction yielded high-quality concave Pt polyhedral nanocrystals with a yield above 90%. Detailed TEM and SEM characterizations (Figure 6a–h) revealed that these concave nanocrystals were essentially octapods with eight trigonal pyramidal arms. Based on the apex angle of the trigonal pyramidal arms, the exposed facets of the trigonal pyramidal arms are {411}. The octapod structure can be better described by excavating out a tetragonal pyramid from each square (100) face of a cube. Each cut-out pyramid has a square (100) base face and four exposed (411) faces passing through the four corners of the excavated (100) square face. Overall, an octapod particle has 24 identical kite-shaped {411} faces, each of which is composed of two coplanar isosceles triangles with apex angles of 50.5 and 86.6° sharing the same base. The structure of the octapods was also verified by a set of tilted TEM measurements. When octapod crystals were oriented along the [110] zone axis, some of their (411) faces were driven parallel to the TEM beam. Indeed, some (2n-1, 1, 1) steps [e.g., (311), (511)] made of subfacets of (111) and (100) planes were clearly observed (Figure 6i).

An ideal high-index (411) Pt facet is periodically composed of (311) and (511) steps (Figure 6j). A Pt (2n-1, 1, 1) surface consists of an ordered staircase of steps separated by (111) step edges. The corresponding terrace-step notation for a Pt (2n-1, 1, 1) surface is Pt (S)-[n(100) × (111)] where n represents the width

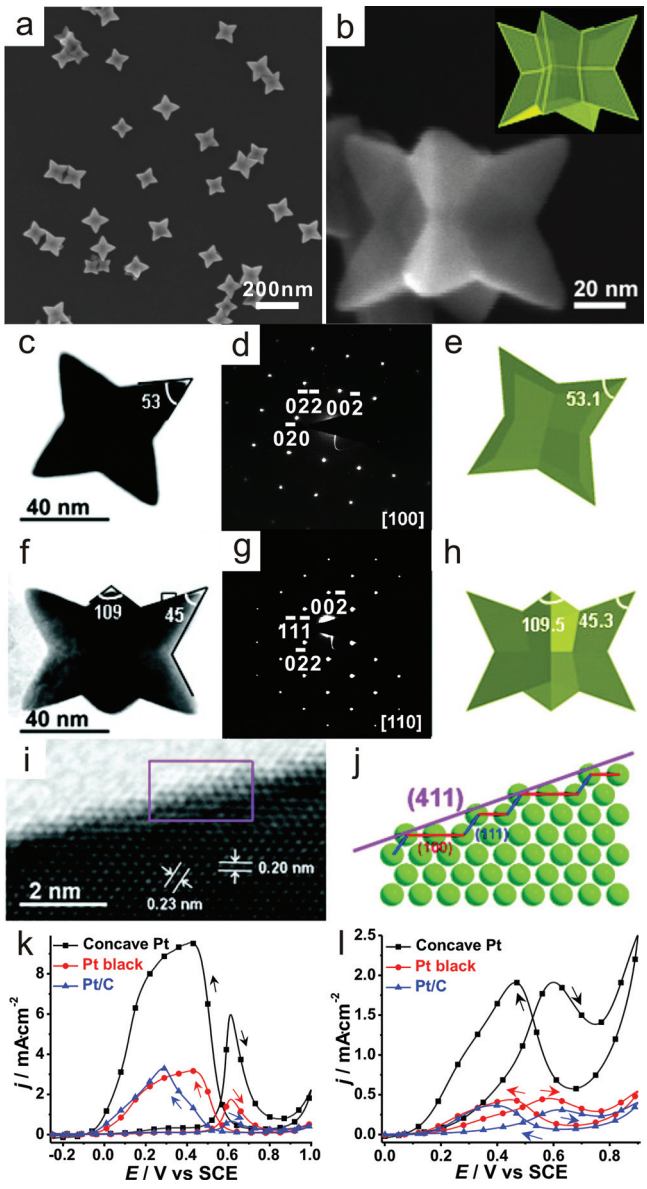

Figure 6. a) SEM image of concave Pt nanocrystals synthesized by reducing H_2PtCl_6 in the presence of methylamine. b) High-magnification SEM image of a single concave Pt nanocrystal, the top insert shows an ideal geometrical model. c,f) TEM images, d,g) SAED patterns, e,h) geometric models. c–e) were oriented along [100] while f–h) along [110]. i) HRTEM image of the region indicated by the box in f). j) Atomic model for the region indicated by the box in i). k,l) CV curves for electro-oxidation of k) formic acid in 0.5 M H_2SO_4 + 0.25 M HCOOH solution at a scan rate of 50 mV/s and l) ethanol in 0.1 M $HClO_4$ + 0.1 M CH_3CH_2OH solution at a scan rate of 50 mV/s. Reproduced with permission from ref. [37], copyright 2011 American Chemical Society.

in the number of (100) terrace atoms. Pt (411) surface has thus a high density of step sites whose coordinated number is only 7. Without other stabilizing factors, these low-coordinated sites should not be stable and would eventually disappear during growth. The strong coordination of amines and therefore stabilizing the low-coordinated atomic sites was proposed as the main contributor to the evolution of high-index {411} facets in the synthesis. The adsorption of methylamine on the surface of the as-prepared Pt octapods was indeed detected by FT-IR spectroscopy.

The essential role of amine in creating high-index Pt facets was verified by the results of the following experiments: (1) The reactions in the absence of amine yielded Pt nanocrystals with mixed morphologies (e.g., cubes, cuboctahedra). (2) When methylamine was substituted with other amines (i.e., ethylamine, butylamine, 4-methylpiperidine, trimethylamine), the reactions also yielded octapods. Even NH_3 led to the formation of the octapods. (3) The perfect Pt octapod nanocrystals were obtained only when the supplied methylamine was larger than a certain amount. Reducing the amount of methylamine produced concave nanocubes, each of which has 24 identical {411} trapezoid facets and 24 identical right-angled isosceles triangle-shaped {100} facets. Together the concavity of the concave nanocubes, the ratio of {100} to {411} facets decreased with increasing amount of amine until the complete disappearance of {100} facets. Since methylamine was the most essential to the formation of concave nanocrystals and supplied at once at the very beginning, the concave feature was observed concomitant with the whole growth process.

Like many other nanocrystals with high-index exposure surfaces,[31,38,62] the as-prepared Pt octapod nanocrystals exhibited enhanced electrocatalysis activities owing to abundant step sites on their {411} facets (Figure 6k,6l). For comparison, the electrocatalysis activities of catalysts were normalized to the electrochemically active surface areas (ECSA). In the electro-oxidation of ethanol, the normalized activity of the Pt octapods was measured to be 4.2 and 6.0 times greater than commercial Pt black and Pt/C, respectively. A similar behavior was found in the electro-oxidation of formic acid in which the octapod nanocrystals showed the best activity, 2.3 and 5.6 times greater than commercial Pt black and Pt/C, respectively. Moreover, the Pt octapods displayed excellent stability during the electrochemical measurements. It should be noted that the electrocatalysis activity of concave nanocubes did increase with the percentage of {411} surfaces until reaching the maximum when they were perfect octapods.

High-index facets of an fcc metal (e.g., Pd, Pt) have high density of low-coordinated surface atoms and therefore are very promising structure for the design of catalysts with significantly enhanced activity. Electrochemical methods have been developed to prepare high-index faceted Pd and Pt nanocrystals on electrodes.[33,62,63] However, the method is not desirable for large-scale synthesis. Recently, the synthesis of many high-index faceted Au nanocrystals has been achieved by wet chemistry.[13–16] The wet-chemical synthesis of high-index catalytic facets was also achieved by epitaxial growth Pd and Pt on pre-made high-index Au facets[56,58–61] or by making AuPt alloy.[94] Although pure Pd and Pt concave nanocubes with high-index facets were fabricated,[95–97] their formation mechanisms are still unclear. The facile synthesis of concave Pt octapods fully enclosed by {411} facets using amines as the surface controller further demonstrates the power of small adsorbates in preparing highly catalytically active nanostructures,[37] which could provide as a system to gain deep understanding how molecular adsorbates promote the formation of high-index facets.

5. Evolution from Simple Structures to Complex Morphologies by a Combination of More Factors

As discussed in Section 4, when coupled with a relatively slow reducing rate of the synthesis system, the strong adsorption of different molecules can induce the formation of well-defined nanocrystals having the exposure surfaces where the adsorbate molecules are selectively bound. In the other word, thermodynamically, small adsorbates control only the surface structure but not the morphology of the nanocrystals. However, for many applications, the morphology of nanocrystals could be equally important as their surface structure. For example, when nanocrystals are deposited on conducting substrates to form electrodes for electrochemical studies, the porosity of the electrodes highly depends on the shape of the nanocrystals, which could significantly influence their electrochemical performances because of mass and electron transfer issues. Moreover, the morphology of nanocrystals is critical for many bio-applications simply because cells take up different-shaped nanocrystals differently. Therefore, beyond the surface control, the morphology control of nanocrystals is important. As described in Section 2, for fcc metals such as Pd and Pt, nanocrystals with different morphologies could have the same exposure surface. Under thermodynamic control of strong chemisorption, the synthesis of various morphologies with the same exposed facets is possible.

5.1. Anisotropic Growth of Pd Nanowires under Kinetic Control

In general, different morphologies show different kinetic behaviors during their growth. In order to selectively prepare nanocrystals with a certain morphology, factors of growth kinetics have to be considered. For example, the growth of multiply twinned nanocrystals of fcc metals is under kinetic control. During the growth, the increase of {111} facets of the nanocrystals can counterbalance the extra strain energy produced by twinning. Whereas, if the multiply twinned crystal grows too fast to balance the excessive strain energy, the twinned nanocrystals will be transformed into single crystals to minimize the stain energy.[3]

In the synthesis of Pd nanocubes assisted by adsorption of I^- on {100} facets described above, a close inspection revealed that, besides the production of Pd nanocubes, five-fold twinned nanorods were yielded as the minor and only byproducts (Figure 2f).[45] Structurally, the five-fold twin nanorods are bound by five {100} side surfaces along the <110> direction. Compared with nanocubes fully enclosed with six {100} facets, the two ends of the nanorods were not {100}. With the strong chemisorption of I^- on {100}, the growth of {100} facets is inhibited. With this prohibition, the growth rate of twinned nanorods would be significantly faster than that of nanocubes simply because of the existence of non-{100} facets at the tips of twinned nanorods that are not tightly bound by I^-. The five-fold twin nanorods/nanowires are then the more favorable structures than single-crystalline nanocubes by the growth kinetics. In the system containing strong {100} adsorbates I^-, in order to obtain five-fold twin nanorods/nanowires in a high yield, the reduction rate of Pd(II) precursors has to be significantly decreased in related to the DMF system used for the synthesis of Pd nanocubes.[45]

Experimentally, an aqueous system that contains $PdCl_2$ as the Pd precursor, PVP as the reducing agent and I^- as the surface controller, was chosen to suppress the reduction of Pd(II).[64] PVP is considered as a reducing agent because of its hydroxyl(-OH) group ends.[98] Compared with ethylene glycol and DMF, PVP provides a much weaker reducing capacity, guaranteeing a low reduction rate of Pd (II) during the synthesis. As illustrated in **Figure 7**a, lowering the reduction rate did produce long Pd nanowires as the main products. The nanowires had a uniform diameter of 9.0 nm along their entire length, which was in the range of micrometers. HRTEM and SAED studies (Figure 7b, 7c) confirmed that the nanowires had five {100} side surfaces along the <110> growth direction. While twinned nanowires were generated as the main products, nanocubes were also presented in the reactions. The co-existence of Pd nanowires and nanocubes in the system provided a nice opportunity to study the evolution of these two different morphologies under the strong surface adsorption of I^-. As expected from the structure, the nanowires should have a much faster growth rate under the weak reducing conditions. Indeed, the kinetics studies revealed that before the depletion of Pd(II) precursors, the Pd nanowires grew much faster than nanocubes. The higher growth rate of Pd nanowires than nanocubes was considered as the main cause for the high-yield production of Pd nanowires. However, after complete consumption of Pd(II), observed was the ripening of the nanowires into nanorods with decreasing aspect ratio (Figure 7d–g) and finally to multiply twinned particles upon increasing the reaction time.

Furthermore, as expected from their anisotropic structure that the facets of their sides and tips are different, the as-prepared Pd nanowires should exhibit chemically distinguishable reactivities on their tips and sides. The galvanic replacement reaction between Pd nanowires and $HAuCl_4$ was selected to probe such a reactivity difference.[64] As illustrated in Figure 7h, only their tips reacted with $HAuCl_4$ when the nanowires were not carefully washed. However, if the nanowires were separated and purified, the sides (i.e., {100} facets) of the nanowires became highly reactive so that Au nanoparticles grew on the sides (Figure 7i).

Under a relatively weak reduction condition, the preferential growth of nanowires (the kinetic-controlled product) over nanocubes (the thermodynamic product) was achieved by using the strong adsorbate (I^-) as the surface controller. This success implies that the reduction kinetics is critical to the shape control of nanocrystals under the surface confinement of strong adsorbates. In the other word, although the strong and specific adsorption of a certain small adsorbate limited the type of surfaces that can be produced, the control over the reduction kinetics of the metal precursors could provide an alternative vector to enrich the morphology of the nanocrystals for many desired applications.

5.2. Etching Growth of Pd Nanocorolla under Surface Confinement

As discussed in Section 3, etching growth is an important factor for morphology control. What can be achieved if etching growth meets the method of using small adsorbates to control

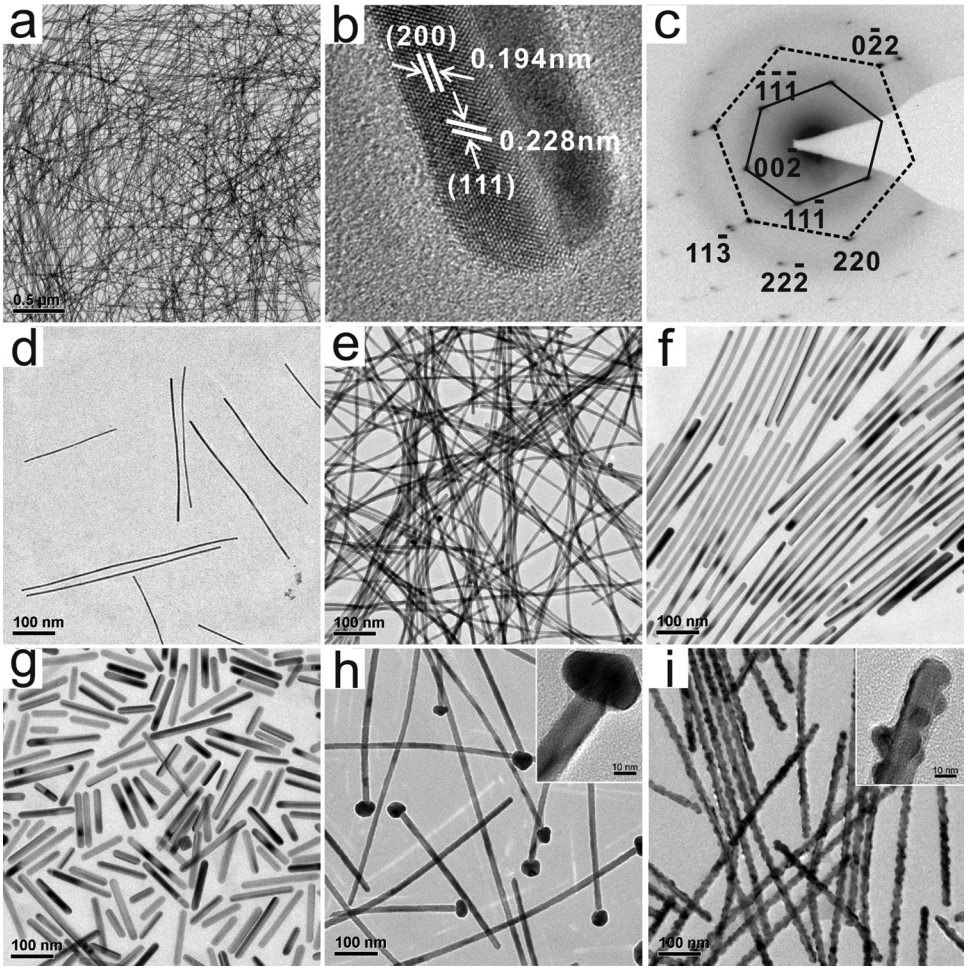

Figure 7. TEM images of Pd nanowires. a) Pd nanowires prepared in DMF, with $PdCl_2$ as precursor and PVP as reductant in presence of I^- in a 2-h reaction. b) HRTEM image and c) SAED pattern of an individual nanowire. d–g) Products obtained in different reaction time: d) 1.5-, e) 2.0-, f) 4.0-, g) 8.0-h reactions. h,i) Au-Pd nanostructures obtained by the reaction between $HAuCl_4$ and Pd nanowires before h) and after i) the nanowires separated from the reaction media after 4 hours. Reproduced with permission from ref. [64], copyright 2009 American Chemical Society.

the surface structure of nanomaterials? To answer this question, a trace amount of Fe^{3+} was introduced into the synthesis of Pd nanosheets using CO as the surface confining agent.[65] With the introduction of Fe^{3+}, as shown in **Figure 8**a and 8b, the obtained Pd nanostructures were corolla-like mesocrystals consisting of connected ultrathin (1.8-nm-thick) Pd nanosheets, significantly from the individual nanosheets prepared in the presence of only CO. The secret for manufacturing the corolla-like Pd mesocrystals (CPdMs) lay in no other than a surface-confined etching growth. While the strong binding of CO on Pd (111) surface as mentioned previously confined the ultrathin sheet-like branches to have (111) surface as the main exposed surface, a trace amount of Fe^{3+} was used to etch Pd seeds. Fe^{3+} has been documented as oxidative etchant for metallic Pd.[54] The driving force for this Fe^{3+} etching growth was the higher redox potential of Fe^{3+}/Fe^{2+} (0.771 V) than that of $Pd(acac)_2$/Pd, $acac^-$ (0.149 V). Oxidative etching by Fe^{3+} on the formed Pd nanosheets created new growing sites for the branched structure. Through oxidative etching, Fe^{3+} could also retard the reduction of Pd(II) precursors to control the size of the Pd mesocrystals. Both the average size of CPdMs and the number of branches of each CPdM increased with increasing amount of Fe^{3+} supplied in the synthesis. It should be noted that in the literature, branched Pd nanocrystals were also obtained prepared when Cu^{2+} was incorporated in the synthesis.[99]

Mesocrystals are single crystal-like superstructures made up of highly ordered crystalline subunits, which serve as structural bridges between nanoscale materials and the macroscale matters.[100] The obtained mesocrystals of Pd nanosheets have the following two important structural features: 1) They consist of ultrathin Pd nanosheets; 2) The Pd nanosheets in each particle are unidirectionally aligned, well spaced but connected to give intraparticular void and increased apparent thickness as compared to individual Pd nanosheets. As a result, CPdMs nicely inherit the unique properties of individual Pd nanosheets: 1) a well-defined surface plasmon resonance absorption feature in the NIR region (Figure 8c); 2) a high electrochemically active surface area; 3) a significant photothermal effect using a NIR laser (Figure 8d). More importantly, owing to the increased apparent thickness and the presence of intraparticular voids,

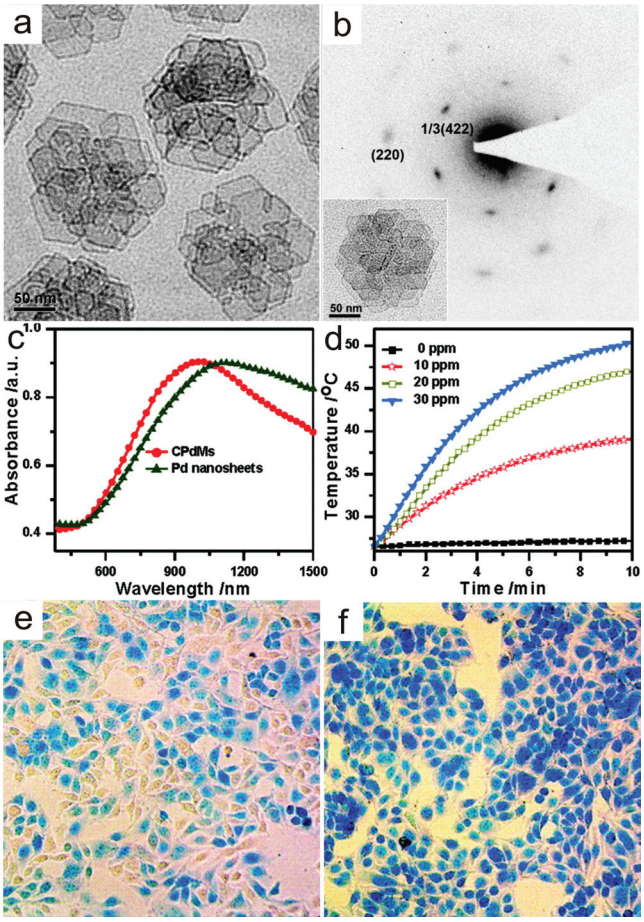

Figure 8. a) Representative TEM image of mesocrystalline Pd nanocorolla obtained in the presence of CO and a trace amount of Fe^{3+}. b) SAED pattern of a single Pd nanocorolla shown in the bottom-left inset. c) Absorption spectra of the Pd nanocorolla and Pd nanosheets. d) Photothermal effect of Pd nanocorolla with different concentration after 10-min-irradiation by a 1-W laser. e,f) Photothermal therapy of cancer cells with Pd nanosheets and Pd nanocorolla respectively, both after 12-h-incubation and then 2-min-irradiation by 808-nm laser in a power density of 1.4 W/cm^2. Reproduced with permission from ref. [65], copyright 2011 American Chemical Society.

the obtained mesocrystals present several advantages over single-domain 1.8-nm-thick Pd nanosheets with a similar dynamic size in solution: enhanced mass transfer in electrochemistry, higher uptaken rate by cancer cells to achieve higher photothermal therapy efficacy (Figure 8e, 8f) and much easier separation by centrifuging. Moreover, the realization of mesocrystalline superstructures makes it possible to increase material surface area without decreasing their particle size. Controlled fabrication of mesocrystals with superstructures is a promising route for obtaining high surface area nanomaterials not just by adjusting the particle sizes.

Have to say, the etching by Fe^{3+} is the key component for controlled formation of CPdMs branched-superstructures; and the ultrathin feature and surface structure of Pd nanosheet branches are well retained under the CO surface confinement. The etching growth under surface confinement strategy makes it possible to control nanocrystals morphology with desired superstructures and exposure surfaces. This example nicely demonstrates that the small adsorbate works very well in coordination with other morphology control factors, and could be widely applied for shape-controlled nanomaterials synthesis. However, more efforts are still needed before the mechanism for CPdMs nucleation and growth is totally revealed. For example, no particles were observed under TEM from the reaction mixture in the first 20 min. While at 25 min, the products found under TEM were already etched at their edges. It is obviously that some critical reactions happened in the first 20 min. A cluster nucleation mechanism is currently proposed for this early stage of etching growth. More techniques have to be applied for directly monitoring the early growth process of CPdMs.

6. Roles of Small Adsorbates Other Than Surface Adsorption in Controlling the Shape of Nanocrystals

In general, small adsorbates that bind strongly on the specific surface of metallic Pd and Pt are also excellent ligands for Pd and Pt cations. For example, halides (X) bind with Pd cations (M) to form stable anionic complexes such as $[Pd(II)X_4]^{2-}$ and $[Pd(IV)X_6]^{2-}$. The stability constants are $10^{16.1}$ and $10^{24.9}$ for $PdBr_4^{2-}$ and PdI_4^{2-}, respectively.[101] The small adsorbates introduced for the surface control could thus significantly alter the reduction kinetics due to their coordination with the precursor. In the synthesis of noble metal nanocrystals, the reduction kinetics has been demonstrated as a very important factor to control the final shape of nanocrystals. Furthermore, during the synthesis, the decomposition of small adsorbates might occur. Depending on the nature of the decomposition products, some might influence the growth of the nanocrystals too. Two examples are given below to illustrate how small adsorbates play important roles other than surface adsorption in the shape control of Pd nanocrystals.

6.1. Hollow PdPt Alloy Nanocubes

As described in Section 4.1, uniform Pd nanocubes were prepared from the mixture containing $Pd(acac)_2$, NaI and PVP in DMF. What's more was that, if half of $Pd(acac)_2$ was replaced by $Pt(acac)_2$, the reaction yielded uniform hollow PdPt nanocubes (**Figure 9**a).[45] As revealed EDX line scanning profile across single PdPt nanocubes (Figure 9b), the as-obtained hollow nanocubes were single-crystalline alloy nanocrystals with both Pd and Pt homogeneously distributed in them. The molar ratio of Pd/Pt was ~1, close to that supplied. The void space inside each hollow PdPt nanocube was through-connected with its external surface, leading to increased accessible surface area of the nanocubes. As a result, the hollow nanocubes showed the electrocatalytic activity twice as high as that of the solid cubes in formic acid oxidation (Figure 9c).

In the literature, hollow metal nanostructures were mainly prepared by the galvanic replacement reactions involving the use of two different metals.[102–104] Typically, the synthesis of hollow metal nanostructures has to be carried out in two

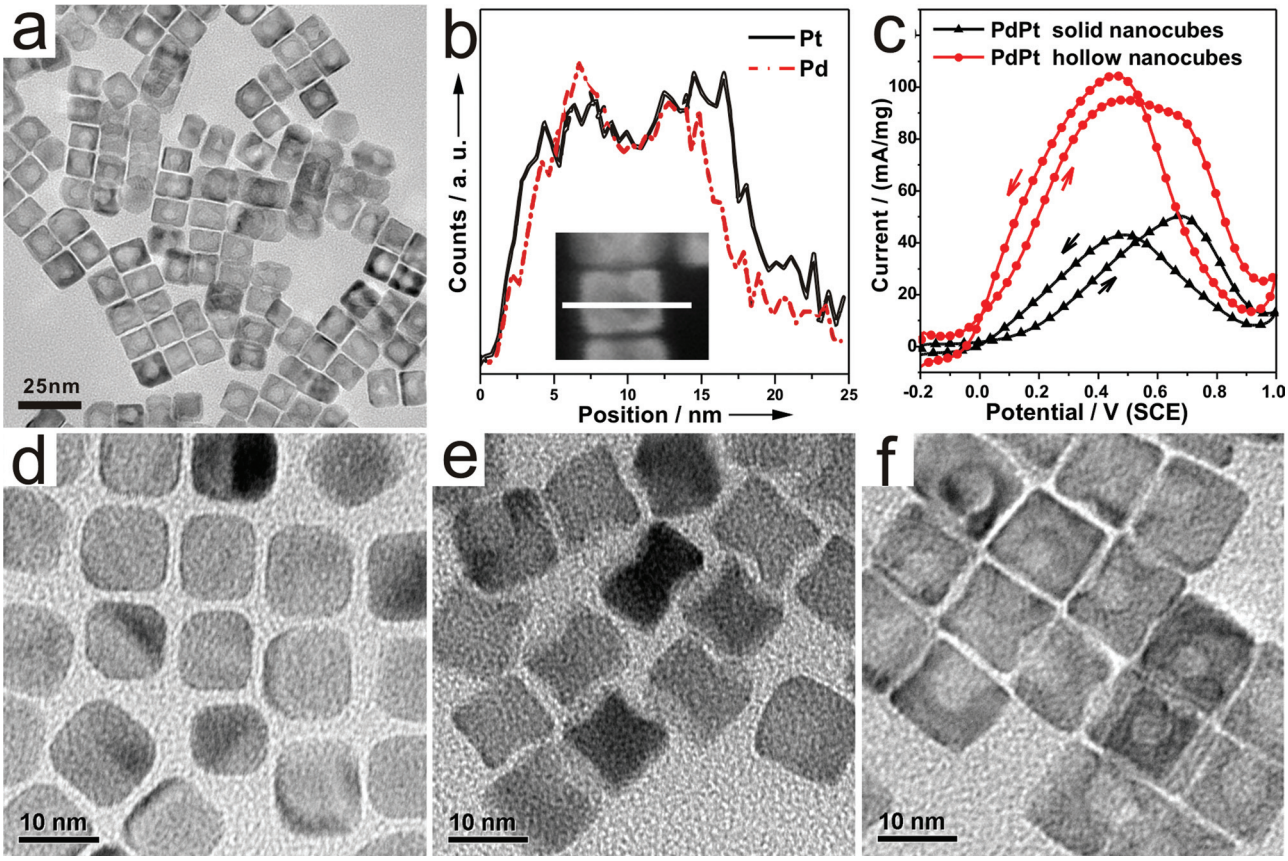

Figure 9. a) TEM image of PdPt hollow nanocubes. b) EDX line-scanning profile across a PdPt hollow nanocube. c) Cyclic voltammetry of PdPt hollow nanocubes and solid nanocubes in 0.5 M H_2SO_4 + 0.25 M HCOOH solution at a scan rate of 50 mV/s. d–f) TEM images of nanoparticles obtained at different reaction times: d) 1 h, e) 2 h, f) 4 h. Reproduced with permission from ref. [45].

separation steps. Solid metallic nanoparticles were first prepared from the first metal cations and then used as the templates for the galvanic replacement with the cations of the second metal. Such a process requires the reduction potential for the first metal pair to be more negative than the second pair. Therefore, by galvanic replacement method, it is considered impossible to obtain hollow structure when the two metal precursors were supplied simultaneously in one pot. For example, the standard reduction potentials (E^0) for Pd(II)/Pd are typically more negative than Pt(II)/Pt pairs in the same coordination environment, the formation of hollow PdPt nanocrystals is not expected from the simple mixture of Pd(II) and Pt(II) with the same ligands coordinated. As expected from the reduction potentials, Pt(II) should get reduced before Pd(II). The galvanic reaction between Pt and Pd(II) would never occur in the system to create the hollow structure. But why hollow PdPt nanocrystals were obtained when I^- was introduced? To have better understanding, the formation process was monitored (Figure 9d–f). The results showed that Pd(II) was reduced to form Pd nanocubes before Pt. The preferential reduction of Pd(II) in the system is mainly due to the different stabilities between $Pd(acac)_2$ and $Pt(acac)_2$ in the presence of I^-. When $Pd(acac)_2$ and $Pt(acac)_2$ were dissolved in DMF with I^-, PdI_4^{2-} and $Pt(acac)_2$ were the actual main precursors for the reactions. It was evidenced that in DMF the reduction of PdI_4^{2-} was more favorable than $Pt(acac)_2$.

It was also revealed that I^- facilitated the galvanic replacement of Pd nanocubes by $Pt(acac)_2$ in the system. In the studies, Pd nanocubes were prepared and purified to remove unbound I^-. The purified Pd nanocubes were then reacted with $Pt(acac)_2$ in a DMF solution of PVP containing different halides. Only in the presence of I^-, the reaction produced uniform hollow nanocubes. No formation of hollow particles was observed from the reactions where I^- was absent or substituted with other halides (i.e., Br^-, Cl^-, F^-). The promoting effect of I^- on the galvanic replacement between Pd nanocubes and $Pt(acac)_2$ can be explained by the strong coordination of I^- to Pd^{2+} and thus fast out-diffusion of Pd atoms for creating the hollow structure. Recently, in presence of Br^-, Xia *et al.* also succeeded the synthesis of PdPt alloy concave nanocubes/nanocages by using Pd nanocubes as sacrificial templates via galvanic replacement as well as a co-reduction process.[105,106] While I^- helped to generate PdPt hollow nanocubes in our system, the presence of Br^- was important in the synthesis of PdPt alloy nanocages. These examples suggest that in the synthesis of Pd and Pt nanocrystals, the small adsorbates introduced for the surface control could play roles other than surface adsorption.

6.2. Concave Pd Polyhedra with Controllable Concavity

In order to study the shape-controlled synthesis of Pd nanocrystals in the presence of small adsorbates as well as a relatively strong reducing agent, we introduced formaldehyde solution to the synthesis system containing $Pd(acac)_2$ and PVP in benzyl alcohol.[39] Interestingly, as shown in **Figure 10**a and 10b, the obtained Pd nanostructures were mainly concave tetrahedra. Both the selected area electron diffraction (SAED) and high resolution TEM (HRTEM) measurements clearly indicated that concave tetrahedra were single-crystalline. As a minor byproduct, the concave trigonal bipyramids were single twinned with stacking fault along the {111} plane. The structure of the concave tetrahedral nanocrystal can be better depicted as an excavated tetrahedron with a trigonal-pyramid excavated at the center of each face of the tetrahedron. Each concave tetrahedra nanocrystal consists of four {111} faces shaped in hollow equilateral triangle and twelve isosceles triangle-like {110} faces concave towards the center of tetrahedron. The outer and inner side length of the hollow equilateral triangle face determines the concave degree of the nanocrystals and therefore the fraction of {110} facets in the as-prepared concave tetrahedra. In addition to TEM and SEM studies, the co-presence of {111} and {110} facets in the concave nanocrystals was confirmed by electrochemical CO stripping measurements. The degree of concavity of the obtained nanocrystals increased with the concentration of formaldehyde supplied in the system. While solid tetrahedra were obtained at the formaldehyde concentration of 0.01 M, concave polyhedra with increasing degree of concavity were produced with increasing concentration of formaldehyde from 0.14 to 0.69 M. With increasing degree of concavity, the percentage of {110} facets gradually increased from 0 to 44% (Figure 10c–e). Electrocatalytic measurements showed that the concave nanocrystals in formic acid oxidation exhibited dependency on the percentage of {110} facets (Figure 10f). The catalytic activity was enhanced with increasing percentage of {110} facets, suggesting that Pd {110} is better surface than {111} for formic acid oxidation.

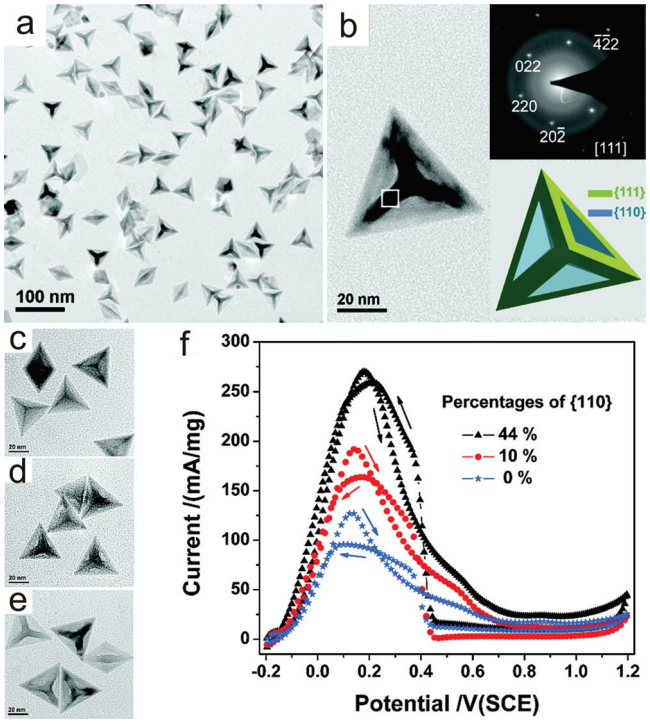

Figure 10. a) Low-magnification TEM image of concave Pd nanocrystals prepared in benzyl alcohol, with $Pd(acac)_2$ as precursor, PVP as capping agent in presence of formaldehyde. b) High-magnification TEM image of a single concave tetrahedron. Top-right and bottom-right insets show the SEAD pattern and the ideal structure model. c–e) TEM images and f) electrocatalytic properties of Pd nanocrystals with different percentages of {110} facets. Reproduced with permission from ref. [39], copyright 2009 American Chemical Society.

Using formaldehyde to tune the reduction rate of the system was our original purpose to have it in the synthesis of Pd nanocrystals. Unexpectedly, the use of formaldehyde yielded the unique concave Pd nanostructures. Although the reason for what is the mechanism behind the formation of the concave nanocrystals is still unclear, we believe that the formation of concave Pd polyhedra is somewhat related to CO adsorption. It has been demonstrated by surface scientists that formaldehyde decomposes on Pd into CO and H_2 easily.[107,108] Before the production of metallic Pd, formaldehyde served as the reducing agent. But once metallic Pd produced, formaldehyde could generate CO for the surface control. As discussed in Section 4.2, the preferential binding of CO on Pd (111) led to the formation of ultrathin Pd nanosheets with {111} as dominating exposure surface. The specific CO adsorption on Pd {111} would help to explain why {111} was the main surface in the concave polyhedra when formaldehyde was used. Very recently, Li *et al.* succeeded in preparing various Pd nanostructures fully enclosed by {111} (i.e., icosahedron, decahedron, octahedron, tetrahedron, and triangular plate) by using formaldehyde as reducing agent in the presence of oleylamine.[109] The combined use of $Na_2C_2O_4$ and formaldehyde led to the formation of PtPd tetrahedral nanocrystals.[70] To fully understand the formation mechanism of concave Pd polyhedra, further studies are still needed to address the question why the concave feature could be created in the presence of formaldehyde. Besides the role as a CO supplier, more factors caused by formaldehyde, particularly kinetic factors, have to be considered.

7. Conclusions and Prospects

7.1. Conclusions

The strong and specific adsorption of small adsorbates on Pd and Pt surfaces has been successfully utilized to control the surface structure of Pd and Pt nanocrystals. To better control the shape of Pd and Pt nanocrystals, slowing down the reduction rate of metal precursors is critical in the design of reactions using small strong adsorbates. Halides strongly adsorb on Pd {100} and thus promote the selective production of Pd nanocubes and Pd nanowires with {100} exposed facets. CO molecules behave differently in the controlled synthesis of Pd and Pt nanostructures. For Pd, CO prefers to adsorb on {111} surface and facilitates the growth of ultrathin Pd nanosheets

having {111} as the main exposure surface. For Pt, the co-adsorption of CO and amine on Pt {100} induces the synthesis of Pt nanocubes.

By using a certain small adsorbate as the surface controller, the morphology of nanocrystals can be enriched by the control over the reduction kinetics or introducing oxidative etching to disturb the growth of seeds. The production of uniform hexagonal ultrathin (1.8-nm-thick) Pd nanosheets in the co-presence of halide and CO serves as a prominent example of how small adsorbates perfectly control the formation of metal nanostructures. Many Pd and Pt nanostructures made by the use of small adsorbates exhibit unique structural features as well as properties that cannot be achieved by other methods.

7.2. Prospects

7.2.1. From Simple Molecules to Complex Molecules

Until now, only a limited number of small adsorbates (i.e., halides, CO, amines) have been clearly demonstrated to play an important role in the surface control of Pd and Pt nanomaterials. The use of these small adsorbates to control the surface structures of noble metal nanomaterials faces the following three problems: 1) Small adsorbates themselves are not bulky enough to prevent the nanocrystals from aggregating during their synthesis. In order to obtain high-quality nanocrystals with well-defined surface structure, bulky capping agents, such as surfactants or polymers, are typically needed in the synthesis. 2) The small adsorbates so far explored are bound on the metal surface with only one binding site although their adsorption configurations might be different. Such a binding situation has sharply limited the number of the accessible surface structures. Although Pt nanocrystals with high-index facets have been made by using amines, the majority of the surface structures that can be controlled by the adsorption method are low-index facets with high coordinated surface atoms. 3) Stronger surface adsorption makes better control over the surface where the small adsorbates are specifically bound. Before the removal of strong adsorbates on their surface, the as-prepared nanocrystals are typically lack of good catalytic activities. Therefore, in order to expand the number of accessible surface structures for structure-property correlation studies, the types of molecules under study have to be expanded. In addition to halide, CO, and monodendate amines that have been studied, carboxylic acids, alkenes, alkynes and multidendate ligands including biomolecules should be considered and may represent a future avenue of research.[110,111]

7.2.2. From Surface Control to Morphology Control

The preferential adsorption of small adsorbates on specific facets of Pd and Pt helps to retain those surfaces during the growth. Even with the use of same adsorbate as the surface controller, as demonstrated in Section 5, it is possible to prepare nanocrystals of different morphologies by the following two strategies: 1) tuning the reduction kinetics to allow the formation of kinetic-control morphologies; 2) using oxidative etching to induce the growth of branched structures. Are there other methods allowing us to further enrich the shape of nanocrystals even when the same small adsorbate is used for the surface control? For instance, it has been demonstrated in the synthesis of both Pd nanosheets and corolla-like Pd mesocrystals where CO controls the formation of Pd {111} facets.[47,65] However, besides the nanosheets, tetrahedra and octahedral are the shapes that also have {111} as the exposed surface. It should be pointed out that, in the synthesis of Pd nanosheets, Pd tetrahedra were also observed occasionally as the minor byproducts. How can we achieve the high-yield production Pd tetrahedra by using CO as the surface controller? Can other shapes of Pd nanocrystals also be synthesized using CO? The successful synthesis of both Pd nanocubes and five-fold twinned Pd nanowires has provided us a very nice example on the importance of reduction rate on the morphology control of nanocrystals when a same adsorbate is used. However, the problem is how we quantitatively evaluate the reduction kinetics of a synthesis system. Many Pd and Pt precursors have rather high absorption coefficients in the UV region. Thus, UV-Vis absorption spectroscopy is a good tool to differentiate the reduction kinetics of different reaction systems. With such a tool, the influence of reduction kinetics on the shape control of Pd and Pt nanocrystals should be systematically studied. Furthermore, structural twinning is an alternative to enrich the morphologies of Pd and Pt nanocrystals and is typically induced by the kinetic control. Seeking for small adsorbates that are able to control the formation of twin boundaries would be beneficial to the synthesis of nanocrystals having complex morphologies but well-defined surfaces.

7.2.3. Understanding How Small Adsorbates Control the Surface Structure

One important guideline to select small adsorbates for effective surface control is to use the small adsorbates that have strong binding affinity with specific Pd or Pt surfaces. However, the interactions of the adsorbates on Pd or Pt surfaces in real syntheses are generally different from those in vacuum that have been widely studied by surface scientists. Usually, trial and error is required to find out what molecular adsorbates act as surface controllers for desired Pd or Pt surfaces. There is lack of theories that enable us to predict the type of surface that be produced by a certain molecule, which is however possible if how molecular adsorbates control the surface is fully understood. To achieve such a goal, the correlation between the molecular adsorbates and the produced surfaces should be extensively studied. The surface binding structures of molecular adsorbates need to be well characterized at the molecular level. The surface control involving the use of CO should be a perfect system for us to start with due to the following reasons: 1) CO molecules have facilitated the synthesis of several unique Pd and Pt nanostructures (e.g., ultrathin Pd nanosheets, Pt nanocubes, Pt-M octahedra);[47,85–87] 2) The binding structure and energies of CO can be identified by IR spectroscopy and also electrochemical CO stripping technique;[71–73,112] 3) The metal surfaces bound by CO can be easily cleaned for reliable surface-dependent properties studies.[75] With no doubt, together with theoretical calculations, full characterizations of CO molecules on the surface of the produced nanostructures will help us to gain insights on how CO molecules control the formation of different nanostructures.

Furthermore, the importance of the chemistry of metallic nanoclusters should be recognized in the controlled synthesis of nanostructures. Many metallic Pd and Pt nanoclusters are able to crystallize into single crystals for total structure determinations.[113–120] Nanocluster chemistry could provide us important information on the adsorption structure of small adsorbates on the metal surface as well as the structure of nanocrystals at the very beginning of the control process. In the synthesis of nanocrystals, such information is usually hard to be acquired but critical to deeply understand how small adsorbates control the formation of nanocrystals.

Acknowledgements

We thank the MOST of China (2011CB932403, 2009CB930703), the NSFC (21131005, 21021061, 20925103, 20871100), the NSF of Fujian Province (Distinguished Young Investigator Grant 2009J06005), the Key Scientific Project of Fujian Province (2009HZ0002-1) and the Fok Ying Tung Education Foundation (121011) for the financial support. We also thank our colleagues who have participated in work cited in this Report, especially Dr. Xiaoqing Huang, Shaoheng Tang, and Dr. Gang Fu.

Received: October 28, 2011
Published online: January 18, 2012

[1] T. K. Sau, A. L. Rogach, F. Jackel, T. A. Klar, J. Feldmann, *Adv. Mater.* **2010**, *22*, 1805–1825.
[2] A. R. Tao, S. Habas, P. D. Yang, *Small* **2008**, *4*, 310–325.
[3] Y. N. Xia, Y. J. Xiong, B. Lim, S. E. Skrabalak, *Angew. Chem. Int. Ed.* **2009**, *48*, 60–103.
[4] R. Gordon, D. Sinton, K. L. Kavanagh, A. G. Brolo, *Acc. Chem. Res.* **2008**, *41*, 1049–1057.
[5] N. Calander, *Curr. Anal. Chem.* **2006**, *2*, 203–211.
[6] A. M. Gobin, M. H. Lee, N. J. Halas, W. D. James, R. A. Drezek, J. L. West, *Nano Lett.* **2007**, *7*, 1929–1934.
[7] E. M. Larsson, C. Langhammer, I. Zoric, B. Kasemo, *Science* **2009**, *326*, 1091–1094.
[8] X. H. Huang, S. Neretina, M. A. El-Sayed, *Adv. Mater.* **2009**, *21*, 4880–4910.
[9] P. K. Jain, X. H. Huang, I. H. El-Sayed, M. A. El-Sayed, *Acc. Chem. Res.* **2008**, *41*, 1578–1586.
[10] S. Lal, S. E. Clare, N. J. Halas, *Acc. Chem. Res.* **2008**, *41*, 1842–1851.
[11] S. E. Skrabalak, J. Y. Chen, Y. G. Sun, X. M. Lu, L. Au, C. M. Cobley, Y. N. Xia, *Acc. Chem. Res.* **2008**, *41*, 1587–1595.
[12] L. Vitos, A. V. Ruban, H. L. Skriver, J. Kollar, *Surf. Sci.* **1998**, *411*, 186–202.
[13] Y. Ma, Q. Kuang, Z. Jiang, Z. Xie, R. Huang, L. Zheng, *Angew Chem Int Ed Engl* **2008**, *47*, 8901–8904.
[14] T. Ming, W. Feng, Q. Tang, F. Wang, L. Sun, J. Wang, C. Yan, *J. Am. Chem. Soc.* **2009**, *131*, 16350–16351.
[15] J. Zhang, M. R. Langille, M. L. Personick, K. Zhang, S. Li, C. A. Mirkin, *J. Am. Chem. Soc.* **2010**, *132*, 14012–14014.
[16] Q. Jiang, Z. Jiang, L. Zhang, H. Lin, N. Yang, H. Li, D. Liu, Z. Xie, Z. Tian, *Nano Res.* **2011**, *4*, 612–622.
[17] G. A. Somorjai, J. Carrazza, *Ind. Eng. Chem. Fundam.* **1986**, *25*, 63–69.
[18] G. A. Somorjai, M. Yang, *Top. Catal.* **2003**, *24*, 61–72.
[19] G. Ertl, *Angew. Chem., Int. Ed.* **2008**, *47*, 3524–3535.
[20] G. A. Somorjai, A. M. Contreras, M. Montano, R. M. Rioux, *Proc. Natl. Acad. Sci. U. S. A.* **2006**, *103*, 10577–10583.
[21] Y. Li, Q. Liu, W. Shen, *Dalton Trans.* **2011**, *40*, 5811–5826.
[22] D. W. Goodman, *Surf. Sci.* **1994**, *299–300*, 837–848.
[23] T. S. Ahmadi, Z. L. Wang, T. C. Green, A. Henglein, M. A. El-Sayed, *Science (Washington, D. C.)* **1996**, *272*, 1924–1926.
[24] S. Mostafa, F. Behafarid, J. R. Croy, L. K. Ono, L. Li, J. C. Yang, A. I. Frenkel, B. R. Cuenya, *J. Am. Chem. Soc.* **2010**, *132*, 15714–15719.
[25] R. Narayanan, M. A. El-Sayed, *Nano Lett.* **2004**, *4*, 1343–1348.
[26] C.-K. Tsung, J. N. Kuhn, W. Huang, C. Aliaga, L.-I. Hung, G. A. Somorjai, P. Yang, *J. Am. Chem. Soc.* **2009**, *131*, 5816–5822.
[27] K. M. Bratlie, H. Lee, K. Komvopoulos, P. Yang, G. A. Somorjai, *Nano Lett.* **2007**, *7*, 3097–3101.
[28] B. Lim, M. J. Jiang, J. Tao, P. H. C. Camargo, Y. M. Zhu, Y. N. Xia, *Adv. Funct. Mater.* **2009**, *19*, 189–200.
[29] Z. M. Peng, H. Yang, *Nano Today* **2009**, *4*, 143–164.
[30] Z. L. Wang, *J. Phys. Chem. B* **2000**, *104*, 1153–1175.
[31] Z. Y. Zhou, N. Tian, J. T. Li, I. Broadwell, S. G. Sun, *Chem. Soc. Rev.* **2011**, *40*, 4167–4185.
[32] N. Tian, Z. Y. Zhou, S. G. Sun, *J. Phys. Chem. C* **2008**, *112*, 19801–19817.
[33] N. Tian, Z. Y. Zhou, S. G. Sun, Y. Ding, Z. L. Wang, *Science* **2007**, *316*, 732–735.
[34] N. Tian, Z.-Y. Zhou, N.-F. Yu, L.-Y. Wang, S.-G. Sun, *J. Am. Chem. Soc.* **2010**, *132*, 7580–7581.
[35] M. L. Personick, M. R. Langille, J.-A. Zhang, C. A. Mirkin, *Nano Lett.* **2011**, *11*, 3394–3398.
[36] T. T. Tran, X. Lu, *J. Phys. Chem. C* **2011**, *115*, 3638–3645.
[37] X. Q. Huang, Z. P. Zhao, J. M. Fan, Y. M. Tan, N. F. Zheng, *J. Am. Chem. Soc.* **2011**, *133*, 4718–4721.
[38] Z. Y. Zhou, N. Tian, Z. Z. Huang, D. J. Chen, S. G. Sun, *Faraday Discuss.* **2008**, *140*, 81–92.
[39] X. Q. Huang, S. H. Tang, H. H. Zhang, Z. Y. Zhou, N. F. Zheng, *J. Am. Chem. Soc.* **2009**, *131*, 13916–13917.
[40] C. J. Murphy, T. K. San, A. M. Gole, C. J. Orendorff, J. X. Gao, L. Gou, S. E. Hunyadi, T. Li, *J. Phys. Chem. B* **2005**, *109*, 13857–13870.
[41] Y. G. Sun, Y. N. Xia, *Science* **2002**, *298*, 2176–2179.
[42] S. E. Habas, H. Lee, V. Radmilovic, G. A. Somorjai, P. Yang, *Nat. Mater.* **2007**, *6*, 692–697.
[43] H. Song, F. Kim, S. Connor, G. A. Somorjai, P. D. Yang, *J. Phys. Chem. B* **2005**, *109*, 188–193.
[44] Y. J. Xiong, H. G. Cai, B. J. Wiley, J. G. Wang, M. J. Kim, Y. N. Xia, *J. Am. Chem. Soc.* **2007**, *129*, 3665–3675.
[45] X. Q. Huang, H. H. Zhang, C. Y. Guo, Z. Y. Zhou, N. F. Zheng, *Angew. Chem. Int. Ed.* **2009**, *48*, 4808–4812.
[46] Y. Zhang, M. E. Grass, J. N. Kuhn, F. Tao, S. E. Habas, W. Huang, P. Yang, G. A. Somorjai, *J. Am. Chem. Soc.* **2008**, *130*, 5868–5869.
[47] X. Q. Huang, S. H. Tang, X. L. Mu, Y. Dai, G. X. Chen, Z. Y. Zhou, F. X. Ruan, Z. L. Yang, N. F. Zheng, *Nat. Nanoetch.* **2011**, *6*, 28–32.
[48] J. Chen, T. Herricks, M. Geissler, Y. Xia, *J. Am. Chem. Soc.* **2004**, *126*, 10854–10855.
[49] B. Wiley, T. Herricks, Y. Sun, Y. Xia, *Nano Lett.* **2004**, *4*, 1733–1739.
[50] M. J. Mulvihill, X. Y. Ling, J. Henzie, P. D. Yang, *J. Am. Chem. Soc.* **2010**, *132*, 268–274.
[51] B. J. Wiley, Y. Chen, J. McLellan, Y. Xiong, Z.-Y. Li, D. Ginger, Y. Xia, *Nano Lett.* **2007**, *7*, 1032–1036.
[52] B. J. Wiley, Y. Xiong, Z.-Y. Li, Y. Yin, Y. Xia, *Nano Lett.* **2006**, *6*, 765–768.
[53] H. Zhang, X. H. Xia, W. Y. Li, J. Zeng, Y. Q. Dai, D. R. Yang, Y. N. Xia, *Angew. Chem. Int. Ed.* **2010**, *49*, 5296–5300.
[54] Y. J. Xiong, J. M. McLellan, J. Y. Chen, Y. D. Yin, Z. Y. Li, Y. N. Xia, *J. Am. Chem. Soc.* **2005**, *127*, 17118–17127.
[55] F. R. Fan, D. Y. Liu, Y. F. Wu, S. Duan, Z. X. Xie, Z. Y. Jiang, Z. Q. Tian, *J. Am. Chem. Soc.* **2008**, *130*, 6949–6951.
[56] C.-L. Lu, K. S. Prasad, H.-L. Wu, J.-a. A. Ho, M. H. Huang, *J. Am. Chem. Soc.* **2010**, *132*, 14546–14553.

[57] T. K. Sau, A. L. Rogach, *Adv. Mater.* **2010**, *22*, 1781–1804.
[58] Y. Yu, Q. Zhang, B. Liu, J. Y. Lee, *J. Am. Chem. Soc.* **2010**, *132*, 18258–18265.
[59] F. Wang, C.-H. Li, L.-D. Sun, H.-S. Wu, T. Ming, J.-F. Wang, J. C. Yu, C.-H. Yan, *J. Am. Chem. Soc.* **2011**, *133*, 1106–1111.
[60] L. Zhang, W. Niu, Z. Li, G. Xu, *Chem. Commun.* **2011**, *47*, 10353–10355.
[61] F. Lu, Y. Zhang, L. Zhang, Y. Zhang, J. X. Wang, R. R. Adzic, E. A. Stach, O. Gang, *J. Am. Chem. Soc.* **2011**, *133*, 18074–18077.
[62] N. Tian, Z. Y. Zhou, N. F. Yu, L. Y. Wang, S. G. Sun, *J. Am. Chem. Soc.* **2010**, *132*, 7580–7581.
[63] Z. Y. Zhou, Z. Z. Huang, D. J. Chen, Q. Wang, N. Tian, S. G. Sun, *Angew. Chem. Int. Ed.* **2010**, *49*, 411–414.
[64] X. Q. Huang, N. F. Zheng, *J. Am. Chem. Soc.* **2009**, *131*, 4602–4603.
[65] X. Q. Huang, S. H. Tang, J. Yang, Y. M. Tan, N. F. Zheng, *J. Am. Chem. Soc.* **2011**, *133*, 15946–15949.
[66] A. Carrasquillo, J. J. Jeng, R. J. Barriga, W. F. Temesghen, M. P. Soriaga, *Inorg. Chim. Acta* **1997**, *255*, 249–254.
[67] M. P. Soriaga, J. A. Schimpf, A. Carrasquillo Jr., J. B. Abreu, W. Temesghen, R. J. Barriga, J. J. Jeng, K. Sashikata, K. Itaya, *Surf. Sci.* **1995**, *335*, 273–280.
[68] Q. Yuan, J. Zhuang, X. Wang, *Chem. Commun.* **2009**, 6613–6615.
[69] Q. Yuan, Z. Y. Zhou, J. Zhuang, X. Wang, *Inorg. Chem.* **2010**, *49*, 5515–5521.
[70] A.-X. Yin, X.-Q. Min, Y.-W. Zhang, C.-H. Yan, *J. Am. Chem. Soc.* **2011**, *133*, 3816–3819.
[71] J. Szanyi, W. K. Kuhn, D. W. Goodman, *J. Vac. Sci. Technol., A* **1993**, *11*, 1969–1974.
[72] W. K. Kuhn, J. Szanyi, D. W. Goodman, *Surf. Sci.* **1992**, *274*, L611–L618.
[73] A. B. Anderson, M. K. Awad, *J. Am. Chem. Soc.* **1985**, *107*, 7854–7857.
[74] C. Langhammer, Z. Yuan, I. Zoric, B. Kasemo, *Nano Lett.* **2006**, *6*, 833–838.
[75] M. Hara, U. Linke, T. Wandlowski, *Electrochim. Acta* **2007**, *52*, 5733–5748.
[76] X. Q. Huang, S. H. Tang, B. J. Liu, B. Ren, N. F. Zheng, *Adv. Mater.* **2011**, *23*, 3420–3425.
[77] S. H. Tang, X. Q. Huang, N. F. Zheng, *Chem. Commun.* **2011**, *47*, 3948–3950.
[78] P. F. Siril, L. Ramos, P. Beaunier, P. Archirel, A. Etcheberry, H. Remit, *Chem. Mater.* **2009**, *21*, 5170–5174.
[79] U. Schlotterbeck, C. Aymonier, R. Thomann, H. Hofmeister, M. Tromp, W. Richtering, S. Mecking, *Adv. Funct. Mater.* **2004**, *14*, 999–1004.
[80] T. Redjala, G. Apostolecu, P. Beaunier, M. Mostafavi, A. Etcheberry, D. Uzio, C. Thomazeau, H. Remita, *New J. Chem.* **2008**, *32*, 1403–1408.
[81] Z. Y. Zhang, Q. Niu, C. K. Shih, *Phys. Rev. Lett.* **1998**, *80*, 5381–5384.
[82] C. Wang, H. Daimon, Y. Lee, J. Kim, S. H. Sun, *J. Am. Chem. Soc.* **2007**, *129*, 6974–6975.
[83] J. Zhang, J. Y. Fang, *J. Am. Chem. Soc.* **2009**, *131*, 18543–18547.
[84] S. I. Lim, I. Ojea-Jimenez, M. Varon, E. Casals, J. Arbiol, V. Puntes, *Nano Lett.* **2010**, *10*, 964–973.
[85] B. H. Wu, N. F. Zheng, G. Fu, *Chem. Commun.* **2011**, *47*, 1039–1041.
[86] Y. J. Kang, X. C. Ye, C. B. Murray, *Angew. Chem. Int. Ed.* **2010**, *49*, 6156–6159.
[87] J. B. Wu, A. Gross, H. Yang, *Nano Lett.* **2011**, *11*, 798–802.
[88] J. Zhang, H. Z. Yang, J. Y. Fang, S. Z. Zou, *Nano Lett.* **2010**, *10*, 638–644.
[89] Y. Kang, C. B. Murray, *J. Am. Chem. Soc.* **2010**, *132*, 7568–7569.
[90] Y. H. Xu, J. P. Wang, *Adv. Mater.* **2008**, *20*, 994–999.
[91] K. J. J. Mayrhofer, V. Juhart, K. Hartl, M. Hanzlik, M. Arenz, *Angew. Chem. Int. Ed.* **2009**, *48*, 3529–3531.
[92] K. J. Andersson, F. Calle-Vallejo, J. Rossmeisl, L. Chorkendorff, *J. Am. Chem. Soc.* **2009**, *131*, 2404–2407.
[93] K. J. J. Mayrhofer, K. Hartl, V. Juhart, M. Arenz, *J. Am. Chem. Soc.* **2009**, *131*, 16348–16349.
[94] L. Zhang, J. Zhang, Q. Kuang, S. Xie, Z. Jiang, Z. Xie, L. Zheng, *J. Am. Chem. Soc.* **2011**, *133*, 171174–17117.
[95] T. Yu, D. Y. Kim, H. Zhang, Y. N. Xia, *Angew. Chem. Int. Ed.* **2011**, *50*, 2773–2777.
[96] M. S. Jin, H. Zhang, Z. X. Xie, Y. N. Xia, *Angew. Chem. Int. Ed.* **2011**, *50*, 7850–7854.
[97] J. Zhang, L. Zhang, S. Xie, Q. Kuang, X. Han, Z. Xie, L. Zheng, *Chem.–Eur. J.* **2011**, *17*, 9915–9919.
[98] Y. J. Xiong, I. Washio, J. Y. Chen, H. G. Cai, Z. Y. Li, Y. N. Xia, *Langmuir* **2006**, *22*, 8563–8570.
[99] Y. H. Chen, H. H. Hung, M. H. Huang, *J. Am. Chem. Soc.* **2009**, *131*, 9114–9121.
[100] H. Colfen, M. Antonietti, *Angew. Chem. Int. Ed.* **2005**, *44*, 5576–5591.
[101] L. G. Sillén, J. Bjerrum, *Stability constants of metal-ion complexes. Supplement no. 1*, Chemical Society, London **1971**.
[102] X. W. Lou, L. A. Archer, Z. Yang, *Adv. Mater.* **2008**, *20*, 3987–4019.
[103] G. S. Metraux, Y. C. Cao, R. C. Jin, C. A. Mirkin, *Nano Lett.* **2003**, *3*, 519–522.
[104] K. M. Nam, J. H. Shim, H. Ki, S.-I. Choi, G. Lee, J. K. Jang, Y. Jo, M.-H. Jung, H. Song, J. T. Park, *Angew. Chem. Int. Ed.* **2008**, *47*, 9504–9508.
[105] H. Zhang, M.-S. Jin, H.-Y. Liu, J. Wang, M.-J. Kim, D.-R. Yang, Z.-X. Xie, J.-Y. Liu, Y.-N. Xia, *ACS Nano* **2011**, *5*, 8212–8222.
[106] H. Zhang, M. S. Jin, J. G. Wang, W. Y. Li, P. H. C. Camargo, M. J. Kim, D. R. Yang, Z. X. Xie, Y. A. Xia, *J. Am. Chem. Soc.* **2011**, *133*, 6078–6089.
[107] E. Muller, F. Muller, *Z. Elektrochem. Angew. Phys. Chem.* **1925**, *31*, 41–45.
[108] G. Ertl, J. Tornau, *Z. Phys. Chem.* **1977**, *104*, 301–308.
[109] Z. Q. Niu, Q. Peng, M. Gong, H. P. Rong, Y. D. Li, *Angew. Chem. Int. Ed.* **2011**, *50*, 6315–6319.
[110] L. Y. Ruan, C. Y. Chiu, Y. J. Li, Y. Huang, *Nano Lett.* **2011**, *11*, 3040–3046.
[111] C. Y. Chiu, Y. J. Li, L. Y. Ruan, X. C. Ye, C. B. Murray, Y. Huang, *Nat. Chem.* **2011**, *3*, 393–399.
[112] K. Yoshioka, F. Kitamura, M. Takeda, M. Takahashi, M. Ito, *Surf. Sci.* **1990**, *227*, 90–96.
[113] E. G. Mednikov, M. C. Jewell, L. F. Dahl, *J. Am. Chem. Soc.* **2007**, *129*, 11619–11630.
[114] C. Femoni, F. Kaswalder, M. C. Iapalucci, G. Longoni, S. Zacchini, *Eur. J. Inorg. Chem.* **2007**, 1483–1486.
[115] C. Femoni, F. Kaswalder, M. C. Iapalucci, G. Longoni, M. Mehlstaubl, S. Zacchini, A. Ceriotti, *Angew. Chem. Int. Ed.* **2006**, *45*, 2060–2062.
[116] N. de Silva, L. F. Dahl, *Inorg. Chem.* **2006**, *45*, 8814–8816.
[117] E. G. Mednikov, S. A. Ivanov, I. V. Slovokhotova, L. F. Dahl, *Angew. Chem. Int. Ed.* **2005**, *44*, 6848–6854.
[118] N. T. Tran, L. F. Dahl, *Angew. Chem. Int. Ed.* **2003**, *42*, 3533–3537.
[119] M. Kawano, J. W. Bacon, C. F. Campana, B. E. Winger, J. D. Dudek, S. A. Sirchio, S. L. Scruggs, U. Geiser, L. F. Dahl, *Inorg. Chem.* **2001**, *40*, 2554–2569.
[120] C. Femoni, M. C. Iapalucci, G. Longoni, P. H. Svensson, P. Zanello, F. F. De Biani, *Chem. Eur. J.* **2004**, *10*, 2318–2326.